KERNFORSCHUNGSANLAGE JÜLICH GmbH

Institut für Plasmaphysik
Association EURATOM-KFA

The Resonant Helical Magnetic Limiter

by

G. Fuchs, A. Nicolai,
G.H. Wolf and B. Steffen

Jül - 1820
Dezember 1982
ISSN 0366-0885

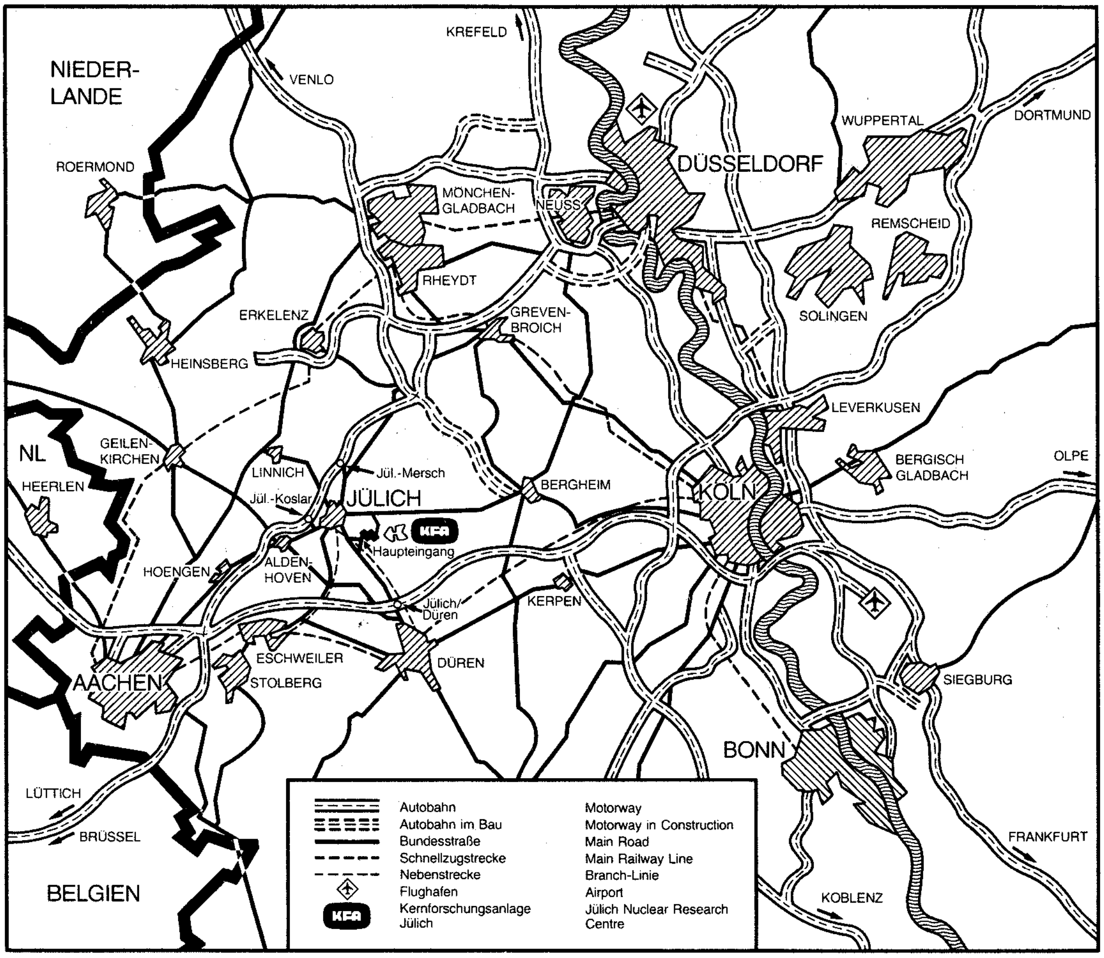

Als Manuskript gedruckt

Berichte der Kernforschungsanlage Jülich – Nr. 1820
Institut für Plasmaphysik Association EURATOM-KFA Jül - 1820

Zu beziehen durch: ZENTRALBIBLIOTHEK der Kernforschungsanlage Jülich GmbH
Postfach 1913 · D-5170 Jülich (Bundesrepublik Deutschland)
Telefon: 02461/610 · Telex: 833556 kfa d

The Resonant Helical Magnetic Limiter

by

G. Fuchs, A. Nicolai,
G.H. Wolf and B. Steffen

The Resonant Helical Magnetic Limiter

G. Fuchs, A. Nicolai and G.H. Wolf
Institut für Plasmaphysik der
Kernforschungsanlage Jülich GmbH,
Association EURATOM-KFA, P.O. BOX 1913,
D-5170 Jülich FRG
B. Steffen
Zentralinstitut für Angewandte Mathematik
der Kernforschungsanlage Jülich GmbH.

Abstract

The physical goals and principles of helical magnetic limiters are described. They are used to develop design criteria for modular structures of helical conductors, which are then applied to a special case (TEXTOR).

A 1-dimensional transport code is used to predict the plasma-parameters for the helical magnetic limiter case. These calculations show a substantial reduction (as compared to a normal limiter case) of the temperatures in the plasma boundary, while the plasma density there stays sufficiently large.

Contents

1. Introduction

The first wall of a fusion machine should be shielded from the impact of energetic particles and the energy flux should be distributed over a large area to prevent local overheating. The core plasma should be screened from those impurities, which are still released. A certain amount of pumping has to be provided in order to remove He-ashes and impurities /1/.

This calls for a boundary engineering to achieve conditions in the boundary layer which are in most respects contrary to what is desired in the plasma core /2/: low temperature, poor particle cofinement, good radial heat conductivity and large radiation losses. Only the plasma density should be as high as possible.

Physical solutions which have been envisaged are the various kinds of divertors, the field line ergodization /3, 4/ and the cold plasma mantle /5, 6/.

The present report examines some further features and aspects of helical magnetic limiters which break up the magnetic surfaces at a distance Δ off the surrounding first wall. It aims at identifying magnetic structures which can be practiced in an experiment and at predicting the plasma parameters to be expected in the boundary layer where the containment is artificially destroyed.

A helical magnetic limiter has several respects in common with the bundle- and axisymmetric-divertor. In all the cases the containment region is devided from the exhaust region by a surface called the separatrix. On the separatrix there is a stagnation line, where the diverted field component has been compensated by applying a counter field from external conductors. In case of the bundle- and axisymmetric divertor, the required currents are quite large.

The stagnation line may also be a helix closing on itself after a finite number of revolutions. In a tokamak such helices naturally exist on rational q-surfaces, we can select a specific one by following a magnetic field line. By definition this is also a stagnation line and needs not be created by an external field. However, to form a helical limiter or divertor /7/ a small helical multipole field is needed to separate the set of field lines into two sets encircling either the o-point of an island wound around the magnetic axis or the magnetic axis only. In this resonant case the currents needed in the external conductors are small, about 1 % of the plasma current.

This scheme of an helical limiter can be modified to an ergodic limiter by overlapping of islands on different q-surfaces /3, 4/. Another proposal is to rotate the multipole field to give a "wall lapping plasma" /8/. As a further modification we propose a helical expanded boundary (see chap. 2.6).

That a magnetically stochastic boundary can produce a cold plasma mantle /9, 10/ can be seen as follows: For a given total power P to be transported to the wall energy balance in the steady state requires

$$P = A v_{\perp} n k T \qquad (1)$$

where A is the surface area and $v_{\perp}$ the effective flow velocity for energy transport. If n is kept constant then $T \propto v^{-1}$. In a stochastic boundary field lines are inclined towards the wall with average inclination angle ε , and the plasma moving with some fraction f_s of the plasma sound speed v_s along these field lines will aquire a radial velocity

$$v_{\perp c} = \varepsilon f_s v_s \qquad (2)$$

For sufficiently large values of ε the convective losses will exceed the losses caused by diffusion and heat conduction, and hence reduce T if n stays high (see chap. 4).

The concept of a helical limiter was recently tested on a small tokamak /11/. It was found that the duration of the discharge could be extended because a disruption was less likely to occure. This finding is not self evident, because a helical field resonant at the plasma boundary can cause magnetic islands also in the interior and might there couple via positive or negative feed back to tearing modes /12/.

2. Magnetic Island Structures

The geometry of ergodic or stochastic fields is very complicated. The terms are not uniquely defined in the literature. We use the following definitiions.

2.1 Definitions

A field is ergodic or stochastic within a region of the space or a subspace if starting from any point of the region and travelling along the field line any other point of the region can be approached within a distance of a prescribed δ , i.e. each field line is dense within the region.

The field is ergodic if the mapping of the region along field lines is continuous.

The field is stochastic within a region, if the mapping of any subregion within that region is discontinuous somewhere along the field lines.

Examples

The trajectory of a harmonic oscillator in k-dimensions with pairwise irrational frequency ratios (Lissajous figure) gives an ergodic field.

The phase portrait of an anharmonic oscillator (e.g. a pendulum) which is exitated with an appropriate frequency spectrum will give stochastic trajectories /13/.

2.2 Stochastic fields

In a stochastic field originally connected regions can become disconnected as they are transformed along field lines. Fig. 1 gives an example, the reason is overlapping of islands on different flux surfaces. Fig. 2 shows a case where the field is stochastic in a subspace, caused by the presence of several disturbing m, n modes on one q surface. The islands themselves may again contain subislands which will help to break up the magnetic structure.

The transformation along field-lines (mapping) of separated regions can in stochastic fields lead to a mixing of the images. It is this property of mixing which could make stochastic fields in the boundary layer useful to achieve a cold plasma mantle and spread the energy flux equally.

However, we have to be careful:
Any stochastic field can only be distinguished from ergodic or periodic fields, if it is known in the whole region of stochasticity, e.g. if the trajectories repetively intersect a surface and the field is unknown on one side off that surface the distinction cannot be

made. Charged particles cannot penetrate a wall and an observer travelling along with the particles can see the field only on one side off the wall, he therefore is unable to tell whether it is periodic, ergodic or stochastic throughout the region.

This has as a consequence that only a finite amount of plasma mixing can be obtained in the boundary region of a tokamak, i.e. as much as it was obtained before the wall was hit. We will return to this problem after we have learned more about the field structure.

2.3 Cylindrical approximation

Magnetic field lines are to a large extend analogous to particle trajectories in classical mechanics /13/, because they are governed by the same types of differential equations. For a surface function we have an equation similar to the Boltzmann equation ($\varphi \triangleq t$) (written here in the form with Poisson brackets)

$$\frac{\partial \psi}{\partial \varphi} + [\,\psi, H\,] = 0 \qquad (3)$$

The Hamiltonian H for a perturbing field of the form

$$B_r(\vartheta, \varphi) = B_{ro} \sin(m\vartheta - n\varphi) \qquad (4)$$

is similar to the one for particles moving in the potential of a travelling wave, it reads (in cylindrical approximation R$\gg$r):

$$H = \int \iota \, dr + \frac{b_r R}{m} [\cos(m\vartheta - n\varphi) - 1] \qquad (5)$$

where

$$\iota = \frac{RB_r}{rB_\varphi} \quad ; \quad b = \frac{B_r}{B_\varphi}$$

Expanding around the resonant radius r_{mn} and transforming to the coordinate system $m\vartheta' = m\vartheta - n\varphi$, we obtain

$$H' = \int \frac{\partial \iota}{\partial r} \Delta r \, dr + \frac{b_r R}{m} [\cos m\vartheta' - 1] \qquad (6)$$

$$\Delta r = r - r_{mn}$$

In this reference system the field lines caught within the island are those with $H' < 0$. In the dashed coordinate system the value of ϑ' oscillates between the limits $\pm\vartheta_0$, when the field line encircles the o-point of the island. On the separatrix $\cos m\vartheta_0$ reaches the maximum value 1. The island width is then

$$2\Delta r = 2\sqrt{\frac{2Rb_r}{m} \cdot \frac{\partial r}{\partial \iota}} \; . \qquad (7)$$

In analogy to the oscillation time of a particle caught in a wave, the number N of toroidal turns a field line needs to encircle the island o-point is:

$$N = \sqrt{\frac{1}{Rb_r} \frac{\partial r}{\partial \iota}} \; K\left(\sin^2 \frac{m\vartheta_0}{2}\right) \qquad (8)$$

where K is a complete elliptic integral. For the cases we will discuss below this N is about 20.

2.4 Toroidal effects

A disturbing radial magnetic field component displaces a field line from the undisturbed flux surface by the amount

$$\delta r = \int b_r \, ds . \tag{9}$$

In toroidal coordinates (cf. Fig. 3) the line element is:

$$ds = \sqrt{R^2\left(1+\frac{r}{R}\cos\vartheta\right)^2 + r^2\left(\frac{d\vartheta}{d\varphi}\right)^2} \quad d\varphi$$

$$\approx R\left(1+\frac{r}{R}\cos\vartheta\right) d\varphi . \tag{10}$$

With the definitions for b_r and b

$$b_r = \frac{B_r}{B_\varphi} = \left(1+\frac{r}{R}\cos\vartheta\right)\frac{B_r}{B_o} = \left(1+\frac{r}{R}\cos\vartheta\right) b \tag{11}$$

we obtain

$$\delta r \approx R \int \left(1+\frac{r}{R}\cos\vartheta\right)^2 b \, d\varphi , \tag{12}$$

The term with r/R causes resonances at other flux surfaces as we may see already from the simple example $b = b_{mn} \cos(m\vartheta - n\varphi)$. Along a field line in a tokamak ϑ is now a non-linear function of φ. We write

$$\vartheta = \iota(\varphi - \varphi_o) + \sum_{\mu=1}^{\infty} a_\mu \sin \iota\mu(\varphi - \varphi_\mu) . \tag{13}$$

We expand the disturbing field

$$b = \sum b_{m,n} e^{i(m\vartheta - n\varphi)} \quad ; \tag{14}$$

inserting (13) and (14) into (12) and using

$$e^{iz\sin\alpha} = \sum_{n=-\infty}^{\infty} e^{in\alpha} J_n(z)$$

(where J_n are Bessel functions)
we obtain

$$\delta r = R\int \sum b_{mn} [e^{i(m\iota - n)\varphi} \prod_{\nu=1}^{\infty} \sum_{=-\infty}^{\infty} J_\mu (m a_\nu)$$

$$+ \frac{r}{R} \sum_{+-} e^{i(\iota(m \pm 1) - n)\varphi} \prod_{\nu=1}^{\infty} \sum_{\mu=-\infty}^{\infty} J_\mu ((m \pm 1) a_\nu)$$

$$+ \mathcal{O}(\frac{r^2}{R^2})] d\varphi . \qquad (15)$$

The equation can be simplified by taking only those terms, which resonate at the respective flux surface. The problem is finally to choose b_{mn} (r) (determined by the location of the conductors and the currents) which maximize δr on those surfaces where islands are desired and minimize it elsewhere. This has to be done with a secondary, e.g. minimum coil current. The optimization is then valid for one particular combination of current density distribution and the β value of the plasma.

To create islands it is in practice sufficient, to keep the phase of the resonant component almost constant along an undisturbed field line. When the conductors are placed close to the resonant zone this requirement is fulfilled, if they follow in parallel those undisturbed field lines where one wants to create the x- and o-points.

In general conductors chosen according to this procedure will also create islands on several other flux-surfaces. Location and size of such parasitic islands are again determined by equ (15), they are strongest for $m' = m \pm 1$, and can be suppresssed by a special coil which cancels the responsible b_{mn}. Because the required field is given, the method described in /14/ could be used to calculate the conductor configuration. A coil resonating with the particular mode (cf. 3) is in practice sufficient to extinguish it.

2.5 Criteria for the application of stochastic fields

We are now able to give the conditions under which application of stochastic fields in the boundary layer of a tokamak is practical and useful.

One condition is that the radial transport caused by the detoriation of the confining field exceeds the transport due to diffusion. Following /2/ we assume that the disturbed field lines have an average inclination angle towards the wall. The plasma will stream along these field lines with $V_{\parallel}$, which is a fraction of the plasma sound speed /15/. The concept of field detoriation is useful, if $\varepsilon \cdot V_{\parallel} > V_D$ holds (V_D = diffusive velocity). In case of Bohm type diffusion this requires $\varepsilon > 10^{-3}$.

ε can be calculated if we assume that the stochastic field is produced by overlapping of islands and the field line is perturbed mainly by those modes resonating along the trajectory. We can then assume that the field line follows one particular island in those regions where the islands are not overlapping. In the overlapping region a fraction of the field lines is assumed to be exchanged between islands with different mode numbers. ε is then determined by chosing Δr such that overlapping occurs, calculating b_r from equ. (7) and N from equ. (8).

$$\varepsilon \approx \frac{\Delta r_{m\iota} + \Delta r_{m^*\iota^*}}{\pi R f\,(N_{m\iota} + N_{m^*\iota^*})} \qquad (16)$$

whereby arc tg $\varepsilon \approx \varepsilon$, f is the fraction of field lines exchanged between islands on the ι and ι^* "surfaces". For strong overlapping f can be close to 1. For small m, m* i.e. n = 1, n* = 1 one finds $\varepsilon < 10^{-3}$ for reasonable island size. The situation can be improved by increasing m. As seen from equ. (7) and equ. (8) this will decrease N because the required disturbing field is increased. There are limitations to this, because only a finite number of conductors can be placed around the torus (cf. fig. 12), they also have to carry a larger current.

For good confinement e.g. for stellarators $\varepsilon < 10^{-3}$ could significantly increase the radial transport. In tokamaks the anomalous transport is probably caused, by the magnetic field structure being already stochastic in certain regions. Then a field imposed from outside might control the losses.

A furhter condition to be fulfilled is that the stochastic boundary should give advantages as compared to the helical divertor and the helically expanded boundary, which both are technically simpler. These advantages can e.g. be that the thickness of the stochastic layer can be matched to the required scrape-off thickness Δ and that it shows mixing.

We already mentioned that the obtainable degree of mixing is limited. There is a competitive mixing process, which is ordinary diffusion. The difference between the two processes is that diffusion works effectively on small scale structures, whereas stochasticity is most effective on the scale of island sizes.

A good and fast (along a limited length of a trajectoy) mixing can be achieved only by combining both processes (see also /16/) and is most effective for

$$v_\perp / v_D = \varepsilon v / v_D \approx 1 \qquad (17)$$

v_D is the diffusion velocity, however, on the scale $d = \lambda \sin\alpha$ (cf. fig. 5) with $d \ll \Delta$. Using

$$v_D = D \frac{\nabla n}{n} \quad ; \quad \varepsilon = \frac{2 \Delta r}{R \Delta \varphi} \quad ; \quad \lambda = \frac{2 \pi r}{m} \quad ;$$

$$\sin\alpha = \frac{2 \Delta r}{r \Delta \vartheta} \quad ; \quad \lambda \sin\alpha = \frac{4 \pi}{m \Delta \varphi} \; \frac{d r}{d \iota} \quad ;$$

$$\nabla n \approx \frac{\Delta n}{d}$$

we get for the mode number needed to meet the requirement (17)

$$m \approx \frac{8 \pi \Delta r \, n \, v_\parallel}{R (\Delta\varphi)^2 \, D \Delta n} \qquad (18)$$

If we limit $\Delta\varphi = 2\pi/\iota$ we get mode numbers which are unacceptably large unless the diffusion coefficient D is large. This means that there has to be anomaleous diffusion within the island structure in order to make the stochastic boundary practicable. Rechester and Rosenbluth /17/ investigated a transport process where a filiamentation with a scale length in the order of an electron cyclotron radius is considered. Very large mode numbers, are needed to fullfil the requirements under which /17/ can be applied in a boundary region with cold plasma

2.6 Helical expanded boundary

As stated above it is not possible in large tokamaks to produce stochastic fields with $\varepsilon > 10^{-3}$ using small mode numbers. For large mode numbers with their high multipolarity, the conductors must be close to the plasma which means in a reactor, between blanket and plasma. Whether or not this is technically feasible, is an open question.

There is a simple method which uses islands to spread the energy flux over a large surface area. This is explained using Fig. 5 . The plasma diffusing from the core towards the wall enters the island from its broad side. Following a small flux bundle from the long side of the island along field lines the cross section of the bundle will have been transformed as it reaches the short side of the island. This transformation is obvious in fig. 8 where a bundle of 3 x 5 field lines was started near $\vartheta = 0$. It circles counter clockwise around the torus and clockwise around the island center. The deformation is seen in the line to the next point sets. If the wall is placed across the center of the island the flux bundle will intersect the wall over a sizeable poloidal extension. One advantage as compared to concepts where a large fraction of the wall acts as limiter is that the limiting area is less sensitive to plasma positioning.

The number of toroidal turns a field line takes from the broad side of the island to the limiter is $N/4 \approx 5$ for low mode numbers.

For the extended helical boundary low mode numbers can be used, this allows to mount the conductors outside the blanket of a reactor.

2.7 Field line tracing and results

Field line tracting calculations have been done for a variety of cases (see fig.7...10), whereby the coil configurations to produce the helical field, the plasma current distribution and the poloidal β have been changed. Those calculations were done for the geometry of TEXTOR (R = 1,75 m, a = 0,5 m) they are, however, valid for any circular tokamak with the same aspect ratio. Coils with different multipolarities (for details see cap. 3.) to resonate at the flux surfaces with q = 3; 4 and 5 have been used. The pitch angle used to wind the conductors onto the torus was changed and we found that the coil current can be minimized if the conductors follow the field lines in "parallel" (we took the same poloidal angle at a larger radius r). The satellite islands on other flux surfaces tend to be small in that case. In TEXTOR we want to create islands at the q = 4 surface near the plasma boundary and eventually ergodize by mixing them with islands at q = 5 (cf. fig. 8); islands at q = 3 are undesirable because they spoil the containment. By energizing a hexapole resonating at q = 3, these islands can be made to disappear.

For the low β case the current distribution was varied by using the field of a wire on the magnetic axis plus the equilibrium vertical field or the Wobig-Rehker approximation

$$B_{\vartheta} = B_{\varphi}\, \iota(0)\, \frac{r/R}{1+(r/a)^2}$$

(where a is a constant)

The hexapole current needed to compensate the islands on $q = 3$ is somewhat different in both cases because the islands appear at different r. Otherwise the two cases are similar. For the finite β case we used the values of the flux function derived from an equilibrium code* and calculated B_{ϑ} (see /18/). Results are given in fig. 10, showing the case $\beta_{pol} = 1$. The inner flux surfaces are conserved by a proper choice of I_{hex} up to $r\ (\vartheta = 0) = 42$ cm. Beyond this radius there are islands around $q = 4$ and a stochastic region even further outside. With increasing β the islands become more stretched on the outside ($\vartheta = 0$) and fat on the inside. A reactor has probably to be exhausted on its outerside the island shape gives then advantages for the expanded helical boundary concept and disadvantages for the helical divertor and the stochastic boundary.

3. Helical Coils

To form a helical divertor or an ergodized helical limiter the helical conductors need not go all around the torus. The coil arrangements can be modular (cf. fig. 6), which is mandatory for reactor application but also eases many of the engineering problems on smaller size tokamaks.

In principle the modules have the topology shown in fig. 11, whereby the extension in ϑ and φ direction may vary. The distances $d_1 .. d_k$ and the pitch angle can be varied to resonate at a particular flux surface with a particular m,n-mode.

* These calculations of the flux function were done by A. Kaleck.

The simplest possibility is to use one module with k = 1; depending on the current, one can get already sizeable islands, they will, however, appear on several flux surfaces /19/.

A more elaborate system consisting of different multipoles designed such that they could be mounted into the 4 large sections of the vacuum vessel of TEXTOR is shown in fig. 12 ,13 . If the conductors are mounted inside the vacuum close to the plasma the following requirements have to be fulfilled:

a) Compatible to (ultra) high vacuum
b) No voltage differences are exposed to the plasma in order to prevent arcing
c) Bakeable to 500 °C (in TEXTOR).

In the special design /20, 21/ these requirements were met by using bundles of thermo coax cable with copper conductor for the helical windings, ss (or inconel) mantle and ceramic insulation in between. The connections of the helical windings are made within two rings on both ends, where the mantles of the cables are welded into cable shoes and these into the rings. The current feed comes in coaxial form within a bellows mounted onto flanges on the vacuum vessel and on one of the cable shoes.

4. Transport Properties

In this section we use a 1-dim. transport code to predict the plasma parameters in a magnetically stochastic boundary region consistently with those in the core, where closed magnetic surfaces are assumed to exist. Because the model is 1 dimensional we cannot take into account all the details of the complicated magnetic field structure in the stochastic region. Instead we use a simplified model and assume that the stochastic field produces leaks in the flux surfaces because the field lines have an average inclination angle $\bar{\varepsilon}$ towards the wall. This $\bar{\varepsilon}$ is zero in the core where closed flux surfaces exist. In the boundary we try

$$\bar{\varepsilon} = 1 - (1 - (\frac{r - r_s}{d})^{\beta})^{\gamma} \bar{\varepsilon}_{max} \qquad (19)$$

where r_s is the radius of the separatrix, d is the distance between limiter edge and separatrix and are constants. For the present study we used $\beta = 2$, $\gamma = 1$ (cf. fig.14).

4.1 Transport Model

Because of high plasma density and low temperature in the mixed layer the mean free path length is short as compared to the length of a field line encircling the axis of symmetry once. Therefore the mass transport parallel to the magnetic field lines is collision dominated. On the other hand the plasma is collision free with respect to the fast cyclotron gyration, i.e. the condition $\omega_{ci} \cdot \tau_i \ll 1$ holds for both ions and electrons. ω_{ci} is the cyclotron frequency and τ_i the collision time /22/. Hence the parallel transport caused by the magnetic mixing is described by a (subsonic) ion sound flow for the mass transport and by parallel heat conduction /22/ and convection, for the energy transport. The particle and energy flux densities parallel to the magnetic field, Γ, $Q_{e\parallel}$, and $Q_{i\parallel}$ respectively read

$$\Gamma = -M n_e v_s \, \mathrm{sign}\left(\frac{\partial p}{\partial l_\parallel}\right)$$

$$Q_{e\parallel} = -n_e \chi_{e\parallel} \frac{\partial T_e}{\partial l_\parallel} + \frac{3}{2} k T_e \Gamma_\parallel \qquad (20)$$

$$Q_{i\parallel} = -n_i \chi_{i\parallel} \frac{\partial T_i}{\partial l_\parallel} + \frac{3}{2} k T_i \Gamma_\parallel$$

The analogous impurity flux densities are not included, impurities are neglected throughout this paper.

$$v_s = \sqrt{\frac{\gamma_e k T_e + \gamma_i k T_i}{m_i}} \qquad (21)$$

is the local ion sound velocity where the adiabatic constants are given by

$\gamma = 1$ and $\gamma = 5/3$.

M(r) is the Mach number profile accounting roughly for the momentum transfer to the plasma due to the recycling processes and for the viscosity. In this approach we assume M(r) = 0.3 as indicated by divertor experiments /15/. l is the coordinate parallel to the magnetic field.

Only the sign of the pressure gradient parallel to the magnetic field enters equ.(20) because the Mach number accounts already roughly for the hydrodynamics of the flow.

n_e, n_i, T_e, T_i, are the electron density, ion density, electron and ion temperature, respectively, k is Boltzmann's constant. The parallel electron and ion heat diffusivities χ_e, and χ_i are given by /22/.

$$\chi_{e\parallel} = 1.91 \cdot 10^{21} \frac{(kT/eV)^{5/2}}{n_e \cdot cm^3 \Lambda} \; cm^2/s \qquad (22)$$

$$\chi_{i\parallel} = \frac{4.07 \cdot 10^{-2}}{\sqrt{A}} \left(\frac{T_i}{T_e}\right)^{5/2} \chi_{e\parallel} \qquad (23)$$

Λ is the Coulomblogarithm and A the atomic mass (A = 1 throughout this paper).

Using the simplified geometry shown in fig.14 , where e_t, e_r, $e_\parallel$ are the unit vectors in the toroidal, the radial and the parallel directions, respectively, the longitudinal derivative becomes

$$\frac{d}{d l_\parallel} = \varepsilon \frac{d}{dr} \qquad (24)$$

Hence the additional effective radial particle, electron and ion energy flux densities, $_r$, Q_{er}, and Q_{ir} respectively, read

$$\Gamma_r = -\varepsilon \Gamma_\parallel M n_i v_s \, sign(\partial p/\partial r)$$

$$Q_{er} = -\varepsilon^2 \chi_{e\parallel} \frac{n_e \partial T_e}{\partial r} + \frac{3}{2} kT_e \Gamma_r \qquad (25)$$

$$Q_{er} = -\varepsilon^2 \chi_{e\parallel} \frac{n_e \partial T}{\partial r} + \frac{3}{2} kT_e \Gamma_r$$

These flux densities are to be superimposed on the radial flux densities evoked by the perpendicular transport processes. A simple model /23/ is chosen for the perpendicular transport described by the diffusion coefficient $D_\perp$, by the electron and the ion heat diffusivities χ_e, χ_i,

$$\chi_{e\perp} = \frac{5 \cdot 10^{17}}{n_e \, cm^3} \quad \frac{cm^2}{s}$$

$$\chi_{i\perp} = f(\nu_i^*) \, q^2 \, \rho_i^2 \, \nu_{ii} \qquad (26)$$

$$D_\perp / \chi_{e\perp} = 0.25$$

The function f depending on the collisionality ν_i is given in /24/; q is the safety factor, ρ_i the ion cyclotron radius and ν_{ii} the ion - ion collision frequency.

Instead of the neoclassical inward flow /23, 24/ we use the phenomenological inward flow term advanced by Engelhardt et al /25/,

$$\Phi_{ir} = -n(r) \frac{2 D_\perp r}{r_{LIM}} \qquad (27)$$

r_{LIM} is the radius of the limiter edge. The sums of the effective flux densities (25) and the perpendicular flux densities described by the coefficients (26) are inserted into the familiar radial transport equations /23/, which are solved by means of the code SIMTOK /26/.

5. Results

The calculations are based on TEXTOR data: major radius R_o = 175, toroidal field B_φ = 2 T, Plasma current I_p = 475 kA. The radii of the separatrix, the limiter edge and the liner surface are r_S = 40 cm, r_{LIM} = 50 cm and r_{LIN} = 56 cm, respectively. The volume averaged density is $5.5 \times 10^{13}/cm^3$. The influence of the maximum mean inclination angle $_{max}$, of the heating power P_H, and of the inward diffusion term of the plasma parameters in the mixed layer is investigated. The transport model in the limiter shadow region is given in /27/. This model provides consistency between the plasma parameters in the limiter scrape-off layer and those in the mixed layer.

The recycling processes are described by the SPUDNUT-code /28/. 100 % recycling is assumed whereby the energy of the recycled neutral hydrogen atoms is 5 eV. In Table I the following values characterizing the mixed layer and the scrape-off layer are compiled:

1. the electron density n_S and the electron temperature T_{es} at the separatrix;
2. the electron density n_L and the electron temperature T_{eL} at the limiter edge;
3. the electron and ion temperature T_{ic} , T_{ec}, and the electron density n_{ec} at the plasma center;
4. the recycled neutral gas influx Φ_H.

The time at which all these data are obtained is t = 300 ms after start. Except if stated otherwise the inward flow term (27) was used in all cases given below. The main input parameters for the computation are the maximum mean inclination angle ε_{max} and the heating power P_H.

The deposition profile of the additional heating is given in fig. 14. The total power is 4.5 MW assumed to be equally deposited in the electrons and ions. The reason for this rather rough description is that we want to cover neutral injection heating and ion cyclotron resonance heating as well; the sensitivity of the results to the parameters characterizing the additional heating method is not investigated here.

The Ohmic heating power is $P_H \approx 500$ kW in case of pure Ohmic heating and thus small as compared to the additional heating ($P_H = 4.5$ MW).

5.1 Results without additional heating

Table I shows that the central core paramameters are roughly constant

($T_i \approx T_e \approx 550$ eV, $n_e \approx 9 \times 10^{13}/cm^3$).

The electron temperature at the separatrix T_e changes from 183 eV to 120 eV if the maximum mean inclination increases from 0 to 2×10^{-3}. The corresponding temperatures at the limiter edge T_e are 38 eV and 19 eV. Due to the high density the ion temperature almost equals the electron temperature. The reasons for the temperature decrease are the enhanced electron heat conductivity and the enhanced ionization loss which increases from 65 kW to 144 kW. (The recycled flux Φ_H increases from 1.9 to 3.9 kA equivalent).

5.2 Results with additional heating (4.5 MW)

The parameters of the central core at 300 ms, are now $T_{ec} \approx 5900$ eV, $T_{ic} \approx 5200$ eV and $n_{ec} \approx 9 \times 10^{13}/cm^3$ in the average, whereby the temperatures are not saturated.

The weak dependence on ε_{max} emanates from the changes of the density profiles. The electron temperatures T_{es} and T_{eL} corresponding to $\varepsilon_{max} = 0$ and $\varepsilon_{max} = 2 \times 10^{-3}$ are now 1040 eV an 446 eV at the separatrix and 112 eV and 54 eV at the limiter edge.

Although the central core temperatures change rapidly in time, T_{es} and T_{is} are relatively constant in the time interval investigated.

Fig.16 shows the plasma parameters in the mixed layer ($\varepsilon_{max} = 2 \times 10^{-3}$). The density is almost constant and the temperature variation in the outer region (45 cm < r < 50 cm) is small. In the vicinity of the separatrix, however, the temperatures decrease strongly because of the increase of the mean inclination angle.

If ε_{max} is zero, the temperatures decrease linearly from their maximum value ($T_i \approx T_e = 1040$ eV) at the separatrix to the minimum value $T_i \approx T_e = 112$ eV at the limiter edge.

The inward flow term (ϕ_{in}) mainly influences the density profile. In fig.17 and fig.18 the time evolution of the density with and without inward flow is shown. Additional heating is switched on and the maximum mean inclination angle is $\varepsilon_{max} = 2 \times 10^{-3}$. The main feature is that in fig.17 a density plateau ($n_e = 4.5 \times 10^{13}/cm^3$ develops. The central density is almost twice the plateau density.

Fig. 18 shows that at t = 310 ms the density stays almost constant over the total radius. The density decay takes place in the limiter scrape-off region.

In the mixed layer the density profile is flat (cf. fig. 17 and 18). In fig. 18 without inward flow the density in the mixed layer is higher ($5.5 \times 10^{13}/cm^3$) than in fig. 18 with inward flow.

6. Conclusions

We have shown that in a toroidal geometry helical islands can be created locally. They can be used to form a helical divertor, a stochastic boundary or a helical expanded boundary. A modular coil configuration to produce these structures may be the same in all cases, the desired pattern is selected by setting the currents in the different modules. A transport code was used to predict the plasma parameters in the boundary region to be expected under these circumstances. The result is, that a significant reduction of the plasma temperature is obtained there, whereas the density stays sufficiently high to provide for screening and (to a lower degree) for shielding.

P.S.
During the writing of this report it was proposed to use on TEXTOR, as a first step, a localized disturbing field to produce a helical island structure. As stated above islands will then appear also in the plasma core. The intriguing feature of a localized coil system (cf. /29/) is, however, that it can be easily mounted on TEXTOR without dismanteling the machine.

Appendix

Localized perturbation coils

Loclized perturbation coils have advantages from the standpoint of engineeering, because they can (eventually) be inserted through a large porthole, and from the standpoint of access for diagnostics, because they do not block the line of sight onto the plasma at many ports.

Such localized coil systems have been proposed for TEXTOR /29/ and for JET /31/. Their disatvantage is that, because of the multitude of excited modes, also those flux surfaces further inside the plasma, which are responsible for plasma confinement in the bulk region, may be de structed.

A cure against this specific disadvantage could be to apply perturbation fields of high multipole order such that their magnetic field rapidly decays with distance. This can easier be done on big machines like JET, because there is sufficient area to accept the electric current required to produce the perturbing magnetic field.

The effect of localized perturbation coils on the magnetic field structure of a tokamak can be visualiced by the following procedure:

Take a flux bundel, which cuts a poloidal plane (φ_1 = const) before the disturbing multipole in region $\{r, \vartheta\}$. This flux bundle will cut a poloidal plane (φ_2 = const) behind the disturbing multipole in a region $\{r', \vartheta\}$. The transformation from the one region to the other is performed by an aperator B (buckle).

$$\{r', \vartheta'\} = B \cdot \{r, \vartheta\}$$

with

$$B = \begin{Bmatrix} 1 + \frac{1}{r} \int_{\varphi_1}^{\varphi_2} \frac{B_r}{B_\varphi} \, ds_\varphi \, , & 0 \\ 0 & , \; 1 + \frac{1}{r\vartheta} \int_{\varphi_1}^{\varphi_2} \frac{B_\vartheta}{B_\varphi} \, ds_\varphi \end{Bmatrix}$$

B = 1 elsewhere (B_ϑ is the disturbing poloidal field component).

After one toroidal turn the same flux bundle will intersect the plane φ_1 = const in a region

$$\{ r'', \vartheta'' \} = S \cdot B \cdot \{ r, \vartheta \}$$

The operator (shear) describes the us ual transformation in an undisturbed tokamak field and therefore conserves flux surfaces. After k turns

$$\{ r, \vartheta \}^k = (S \cdot B)^k \cdot \{ r, \vartheta \}$$

The result of such procedures is shown in fig. , where for simplicity it was assumed that the $\iota = 1$ surface is disturbed. One might, however, infer from this figure the result to be expected for other values of ι.

As we may assume that the plasma is hot in the core region and cool in the boundary we see that $(S \cdot B)^k$ leads to stratification of the plasma with temperature inversions.

To make uses of this effect, the limiters have to be placed properly. A bad choice would be to run the plasma just after passing the perturbing coil onto a surface, because local loading with hot plasma will result. A better solution is to place limiters into the space between the conductors of the perturbing coils and to guide the plasma flow gradually onto these limiters. This scheme coincides to a large extend with the concept of the helical expanded boundary. An advantage of short perturbing coils is, that they are not as sensitive to the value of ι at the boundary, because a multiplicity of modes is excited.

If the disturbed region is sheared, before it hits the surface a helical divertor can be realized by guiding the plasma arround a leading edge onto pump limiters. The location of these limiters with respect to the perturbing coil(s) depends on ι.

The flow pattern becomes very obscure if a flux bundle passes the perturbing coils for several times $(S \cdot B)^K$, leading to a stochastic pattern.

Although the field intersecting a surface becomes stochastic cf. fig. 8 we cannot infer that the magnetic flux density across a surface chosen somehow arbitrarily within the stochastic region would be uniform. Because the particle and energy fluxes are related to the magnetic flux their density well usually also be non-uniform, the positioning of limiters under these circumstances poses sesvere problems, which are still investigated.

References

/1/ G. Fuchs; Jül-Report 1996 (1980)

/2/ G.H. Wolf; Jül-Report 1966 (1980)

/3/ W. Engelhardt and W. Feneberg, J. Nucl. Mat. 76,77, 518 (1978)

/4/ A.V. Nedospasov and M.Z. Tokar, J. Nucl. Mat 93, 94, 739 (1980)

/5/ F. Engelmann, W.Y. Goedheer, A. Nocertini, F.C. Schüller; Proc. of the Int. Symp. on Plasma-Wall-Interaction, P 627, Jülich (1976) Pergamon Press EUR 57821

/6/ B. Lehnert et.al. Plasma Physics and Contr. Nucl. Fus. Res. III P. 265, Vienna (1976)

/7/ F. Karger and K. Lackner, phys. Lett. 61A, 385 (1977)

/8/ T. Tozima, JAERI - M8390 (1979)

/9/ W. Feneberg, G. Fuchs and G.H. Wolf, Proc. 11 SOFT V2, 1079, Oxford (1980)

/10/ W. Feneberg and G.H. Wolf, Nucl. Fus. 21, 669 (1981)

/11/ Z. Yoshida, K. Okama, M. Nakanishi, Y. Seike, N. Inoue, T. Uchida; IAEA Conf. Baltimore (1982)

/12/ F. Karger; et. al.; 6th Conf. on Plasma Physics and Controlled Nucl. Fus. Res. Berchtesgaden 1976 IAEA-CN-351A-7

/13/ A.B. Rechester and T.H. Stix, Phys. Rev. Lett. 36, 587 (1976)

/14/ W. Dommaschk, Z. Naturforschung 36a, 251, (1981)

/15/ S.J. Fielding, A.J. Wooton, Physica Scripta 23, (1981) 97

/16/ A. Samain, A. Grosman and W. Feneberg; J. Nucl. Mat 111 & 112 408 (1982)

/17/ A.B. Rechester and M.N. Rosenbluth Phys. Rev. Let 40 38 (1982)

/18/ K. Lackner, Comp. Phys. Com 12, 33 (1976)

/19/ K.H. Dippel, Private communication

/20/ P. Dierks, Ingenieurarbeit, Jülich (1981)

/21/ P. Dierks, G. Fuchs, and B. Steffen, 12. SOFT, Jülich (1982)

/22/ S.I. Braginski, Reviews of Plasma Physics, Vol. I, p. 183, Consultant Bureau, New York (1965)

/23/ J.T. Hogan, Nucl. Fus. 21, (1981), 365

/24/ F.L. Hinton, R.D. Hazeltine, Rev. Mod. Phy. 48 (1976), 239

/25/ W. Engelhardt, K. Behringer, G. Fussmann, erhandlungen der Deutschen Physikalischen Gesellschaft, Frühjahrstagung Hamburg vom 23. - 27.03.1981, Vortrag P3

/26/ A. Nicolai, JET Workshop on 1-d Transport Codes and Scrape-off Layers (1981) 103, Culham

/27/ K. Audenaerde, G.A. Emmert, M. Gordinier, UWFDM-259 (1978)

/28/ A. Nicolai, G. Fuchs, J. Nucl. Mater 76/77 (1978/ 556

/29/ H. Belitz, K.H. Dippel, G. Fuchs and G.H. Wolf; EURATOM Tomkamak Programme Workshop, Schliersee 8-10 November 1982

/30/ G. Fuchs, B. Steffen J. Nucl. Mat. 93 & 94 (1980) 252

/31/ P.H. Rebut and K.J. Dietz 12. SOFT Jülich, 1982 Proc. V1 85, Pergamon Press

Fig. 1 Evolution of a stochastic field region by overlapping of islands on different q surfaces

Fig. 2 Evolution of a stochastic field region by mode mixing on one q surface

Fig. 3 Toroidal coordinate system used.

Fig. 4 Detoriation of a flux surface caused y a multipole field and shear

Fig. 5 Schematic of the transport in a helical expanded boundary

Fig. 6 Helical coil system consisting of 1 hexapole, 2 octupoles, and 1 decapole as beeing used for the calculations

Fig. 7 The surfaces (approximated) resulting from the destruction of the tokamak surfaces by 4 octupoles (similar to fig. 6) not optimized to reduce islands at q = 3. The method how to derive the picture is given in /24/

Fig. 8 Stochastic boundary achieved by mixing islands at q = 4 and q = 5. By a proper choice of the coil configuration (cf. fig. 6) the islands at q = 3 almost vanish for the poloidal field used here. This claim is at a first glance not obvious from the picture. Note that for r_{star} = 28 cm (ϑ = 0) the field line returns after 3 subsequent revolutions displaced in counter clockwise direction from the start, wheras this is clockwise for r_{start} = 30 cm. As seen from the numerical data both field lines do not intersect the r = 29 cm surface and stay on two different closed surfaces. A picture as in fig. 7 cannot be obtained for the boundary region, because the field is stochastic.

Fig. 9 Magnetic field structure suitable for a helical divertor. Except for the current in the decapole the data are the same as used in fig. 8

Fig. 10 Magnetic field structure with islands for the case $_{pol} = 1$

Fig. 11 Topology for a modular helical coil hookup.

Fig. 12 Construction drawing of a helical octupole which could be mounted in TEXTOR between the vacuum vessel and the liner

Fig. 13 Cut B-C in fig. 13

Fig. 14 Simplified magnetic field geometry in the mixed layer

Fig. 15 Power deposition profile

Fig. 16 Plasma parameter in the magnetically mixed layer

Fig. 17 Time evolution of the electron density with inward flow ($_{max} = 21o^{-3}$, $P_H = 4.5$ MW)

Fig. 18 Time evolution of the electron density without inward flow ($_{max} = 0$, $P_H = 4.5$ MW)

Fig. 19 Detoriation of a flux surface by a short multipole

Acknowledgement

The authors thank K.H. Dippel, W. Feneberg, H. Kever, and A. Samain for the stimulating disucssions. We are gratefully indebted to H.C. Howe whose transport code had been the bases for the development of the "plasma module" of the code SIMTOK

Plasma parameters at the plasma center the separatrix and the limiter edge (t=300ms)

$\varepsilon_{max} \cdot 10^3$	P_H/MW	T_{e_s}/eV	n_{e_s} cm³/10¹³	$(T_{e_L} \approx T_{i_L})$/eV	n_{e_L} cm³/10¹³	T_{i_c}/eV	T_{e_c}/eV	n_{e_c} cm³/10¹³	Φ_H/kA
0	0.5	183	5.3	38	2.6	529	538	9.4	1.9
	4.5	1040	5.1	112	2.1	5520	5130	9.9	3.0
1	0.5	138	4.7	23	4.2	567	579	8.5	3.2
	4.5	530	4.5	65	4.1	6100	5210	8.7	6.1
2	0.5	120	4.5	19	4.3	576	588	8.4	3.9
	4.5	446	4.5	54	4.2	6120	5196	8.6	7.6

TAB. 1

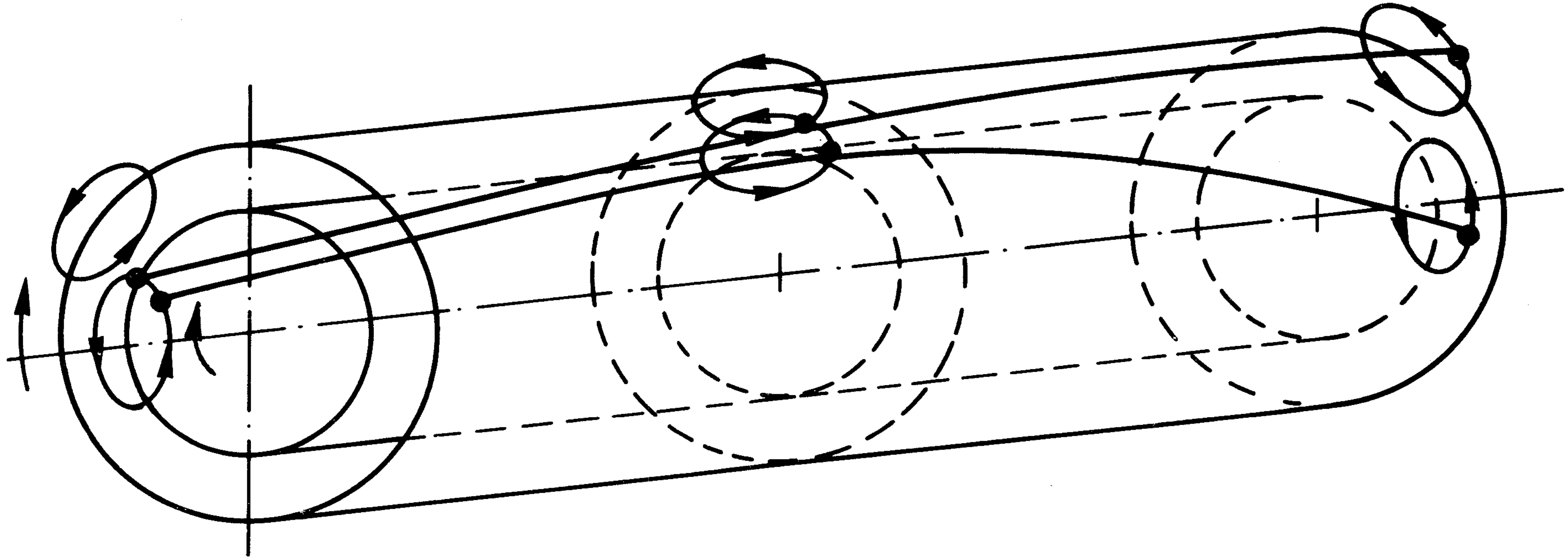

Fig. 1

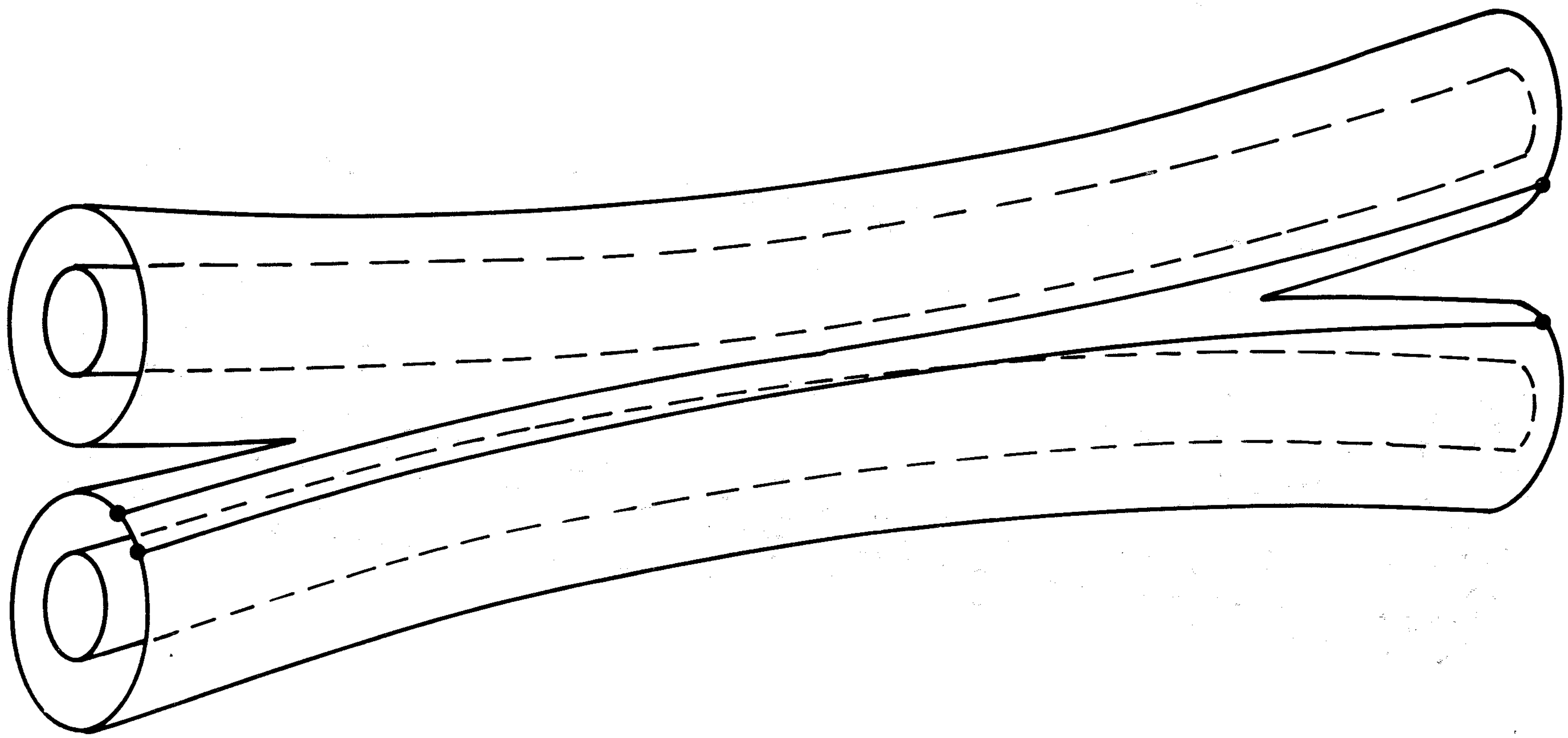

Fig. 2

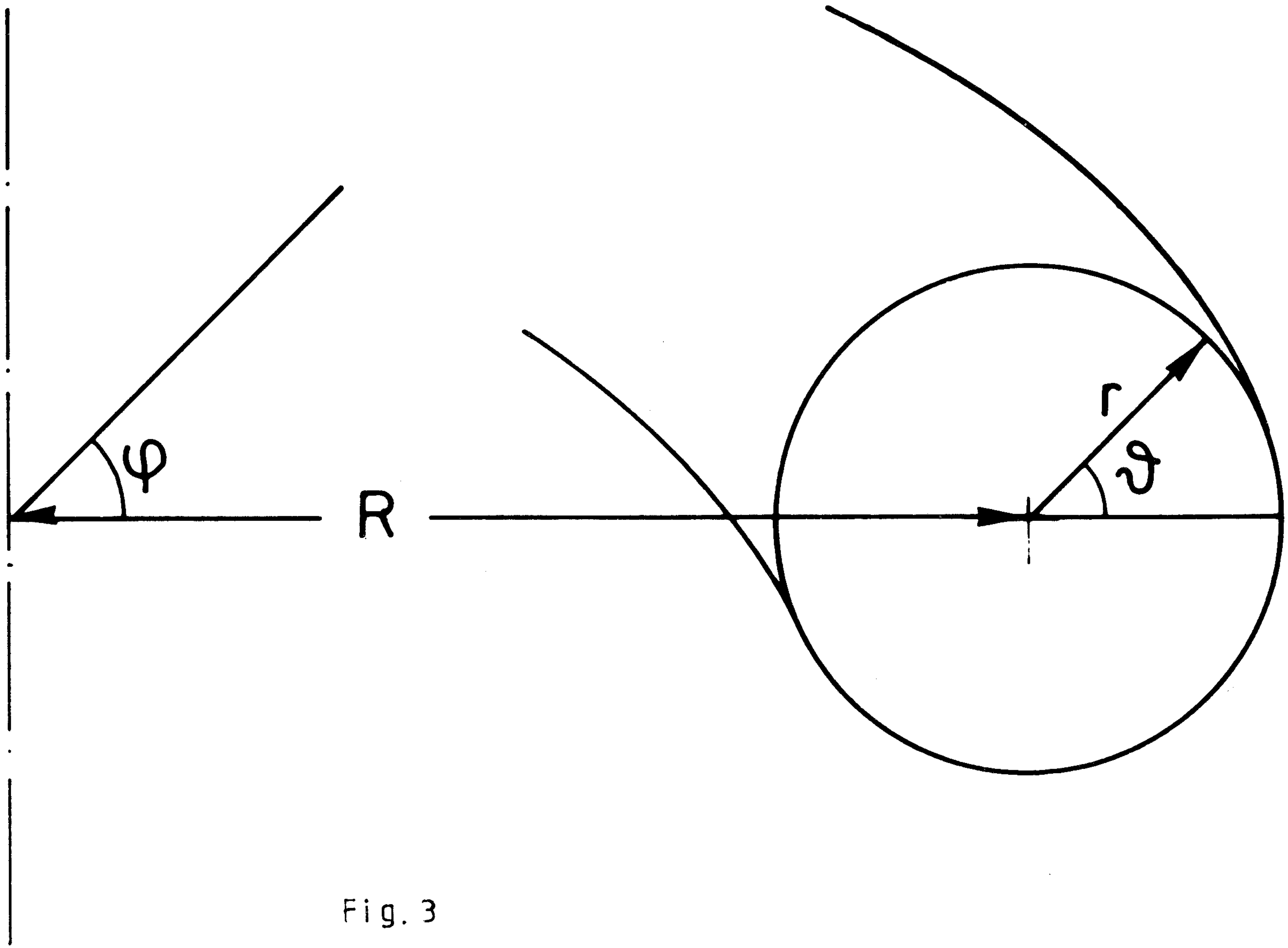

Fig. 3

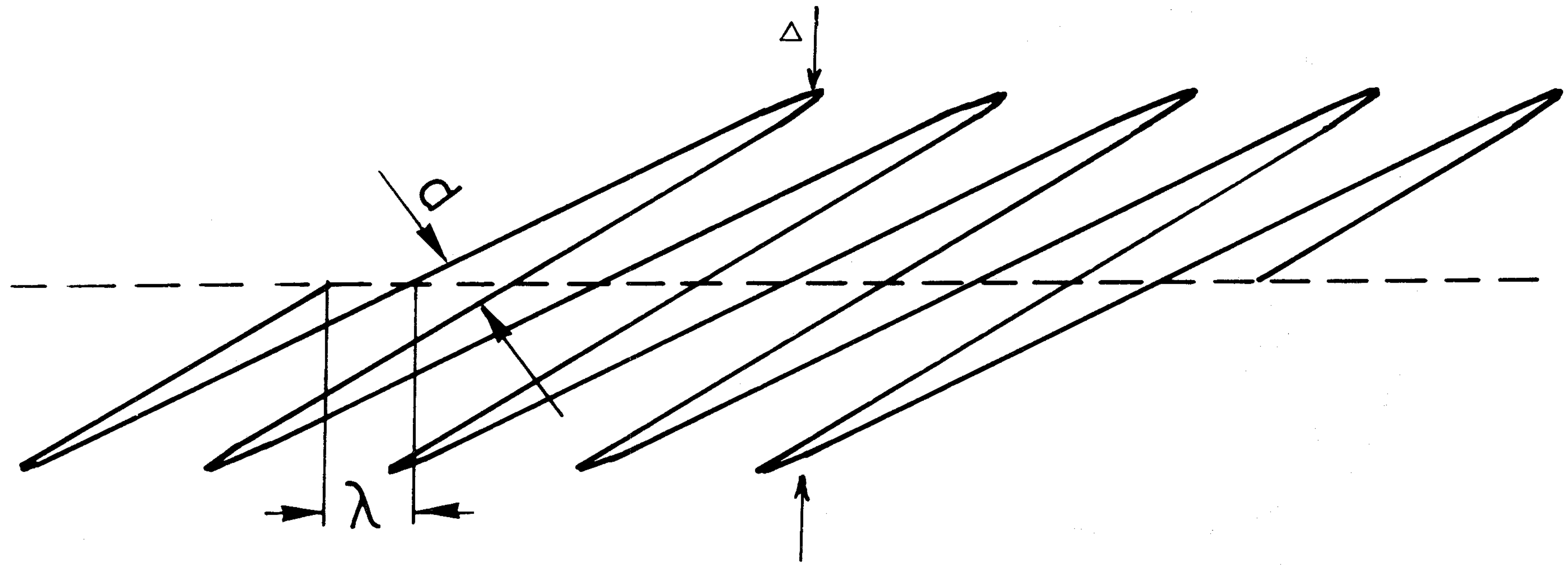

Fig 4

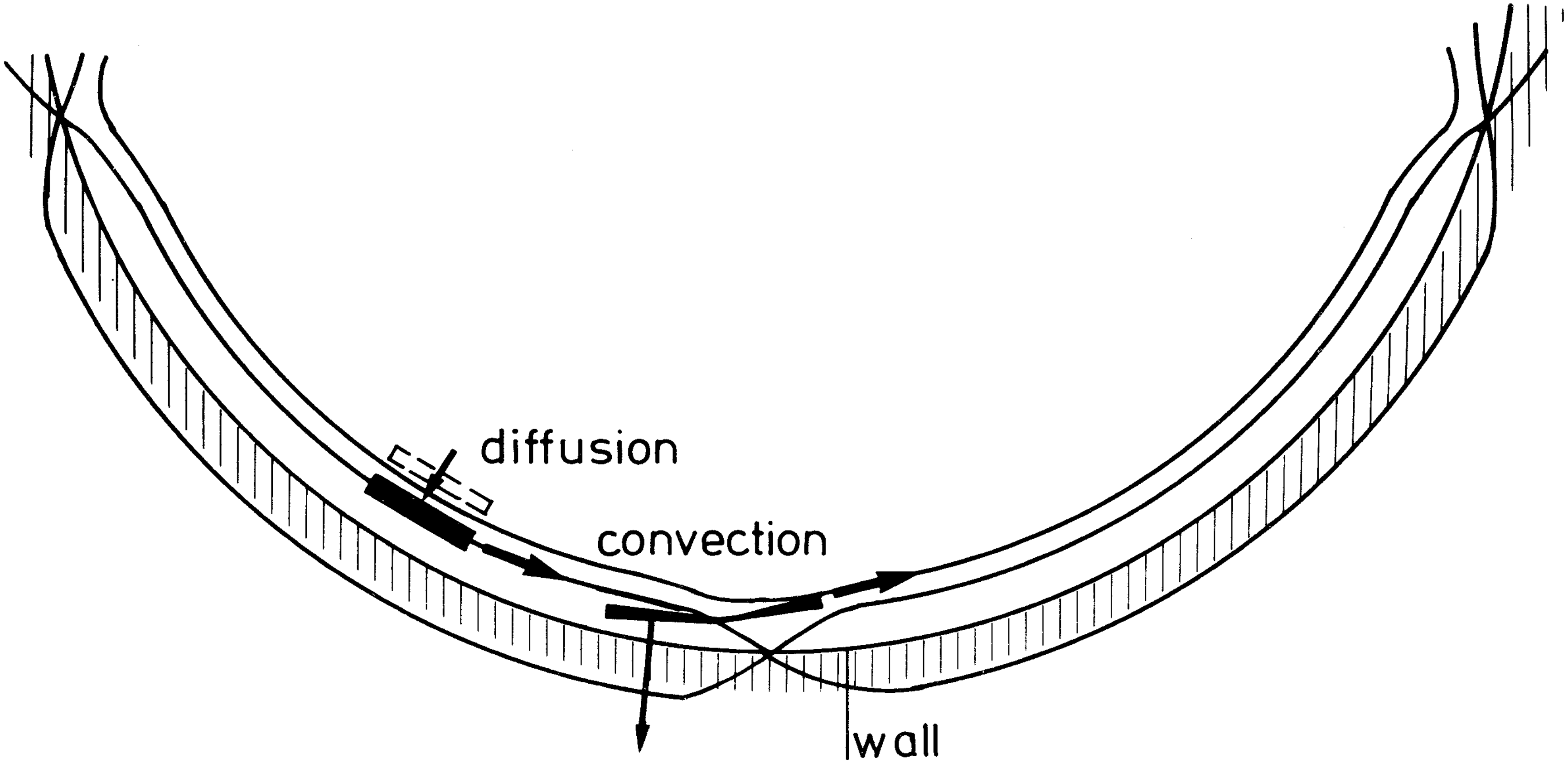

Fig.5

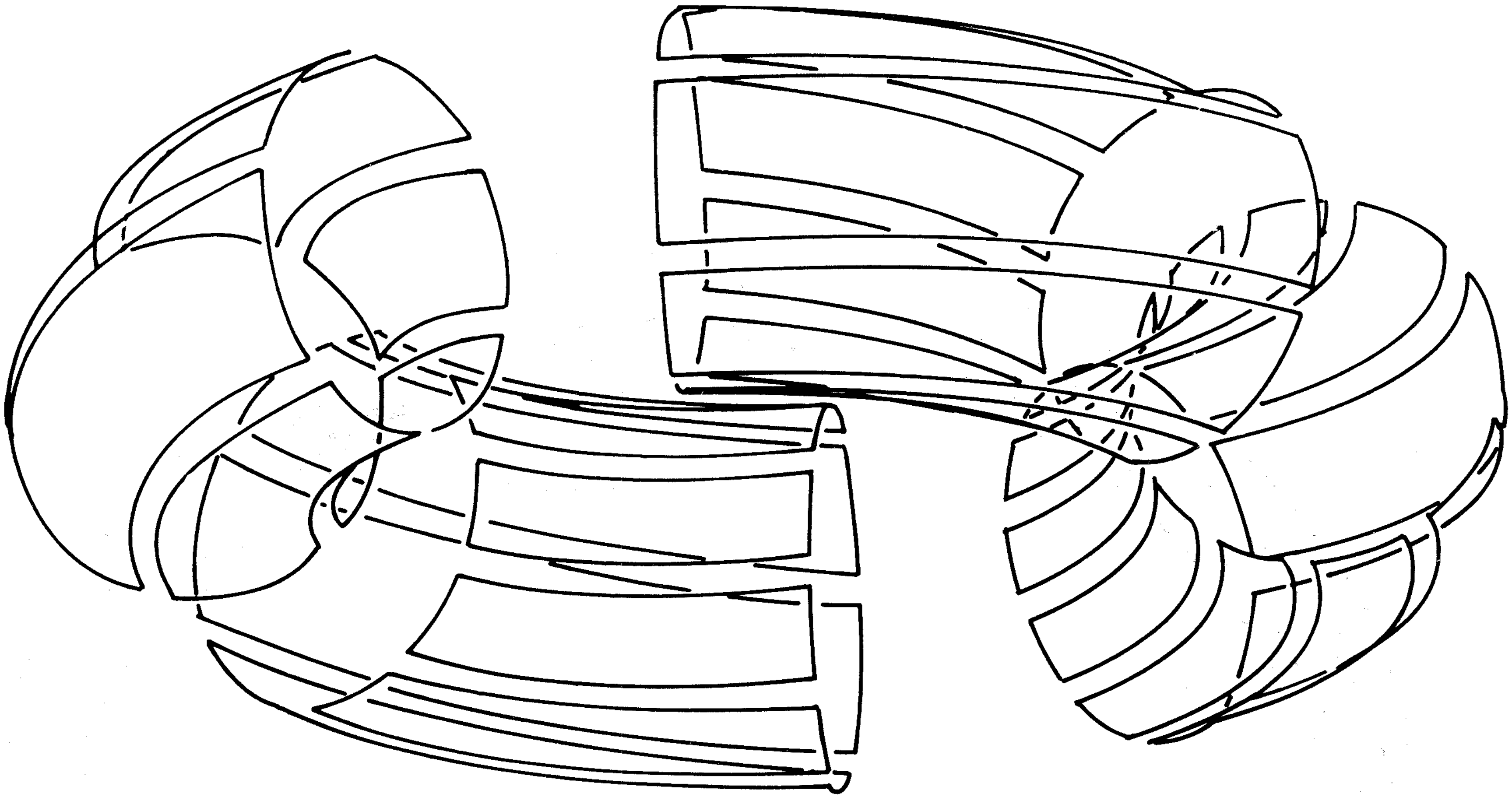

Fig.6

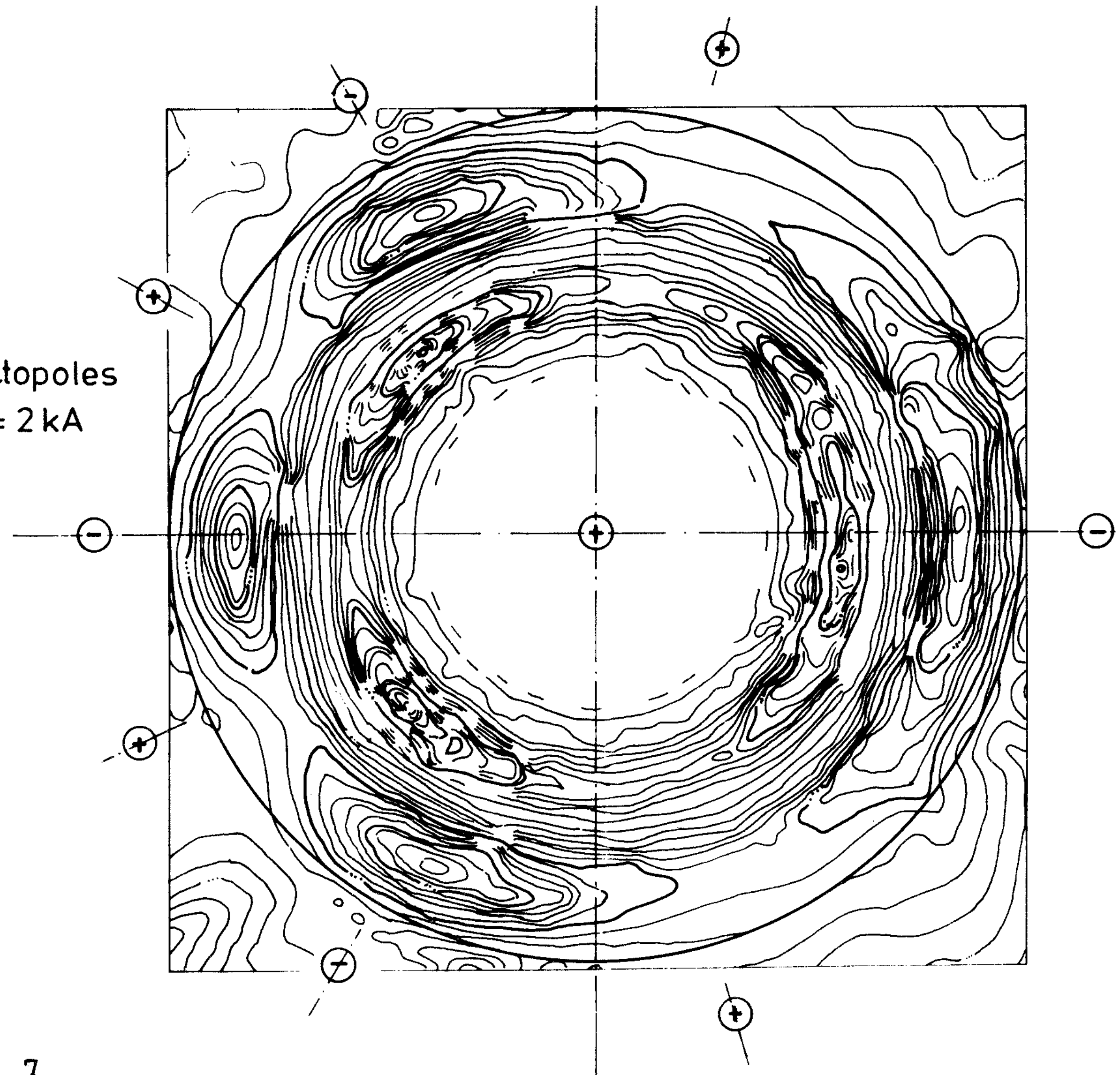

Fig. 7

I_{hel}/kA	hex	oct	dec
	0	4	-4

$r_{start}=28;30;46;48;50$ cm

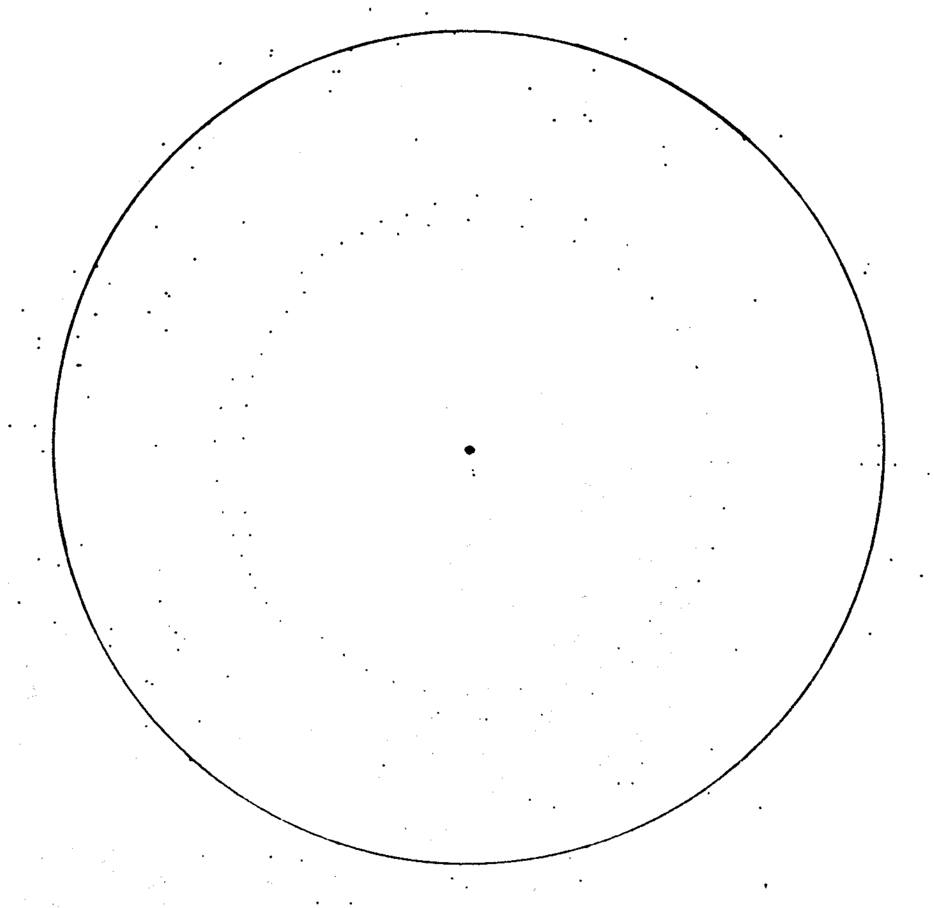

$$B_\vartheta = B_\varphi \iota_0 \frac{r}{R} \frac{1}{1+(\frac{r}{a})^2}$$

Fig. 8

$\frac{I_{hel}}{kA}$	hex	oct	dec
	0	4	2,4

r_{start} = 38; 39; 4o cm

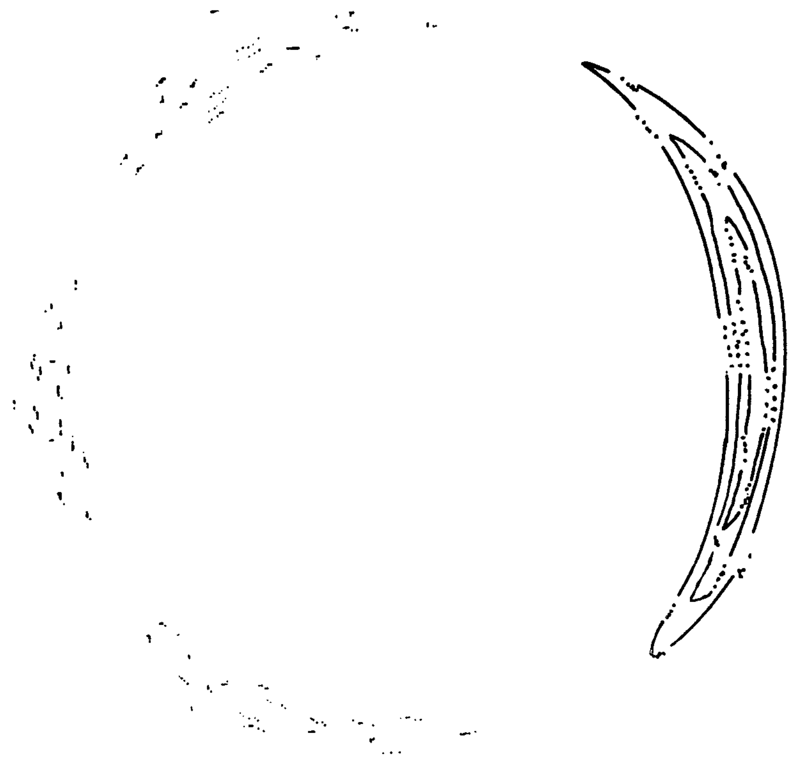

$$B_\vartheta = B_\varphi \, \iota_0 \, \frac{r}{R} \, \frac{1}{1+\left(\frac{r}{a}\right)^2}$$

Fig. 9

$beta_{pol} = 1$

	hex	oct	dec
N	1	2	1
$\frac{I_{hel}}{kA}$	2	4	0

$r_{start} = 32, 34, 36, 40, 42, 44, 46, 48$ cm

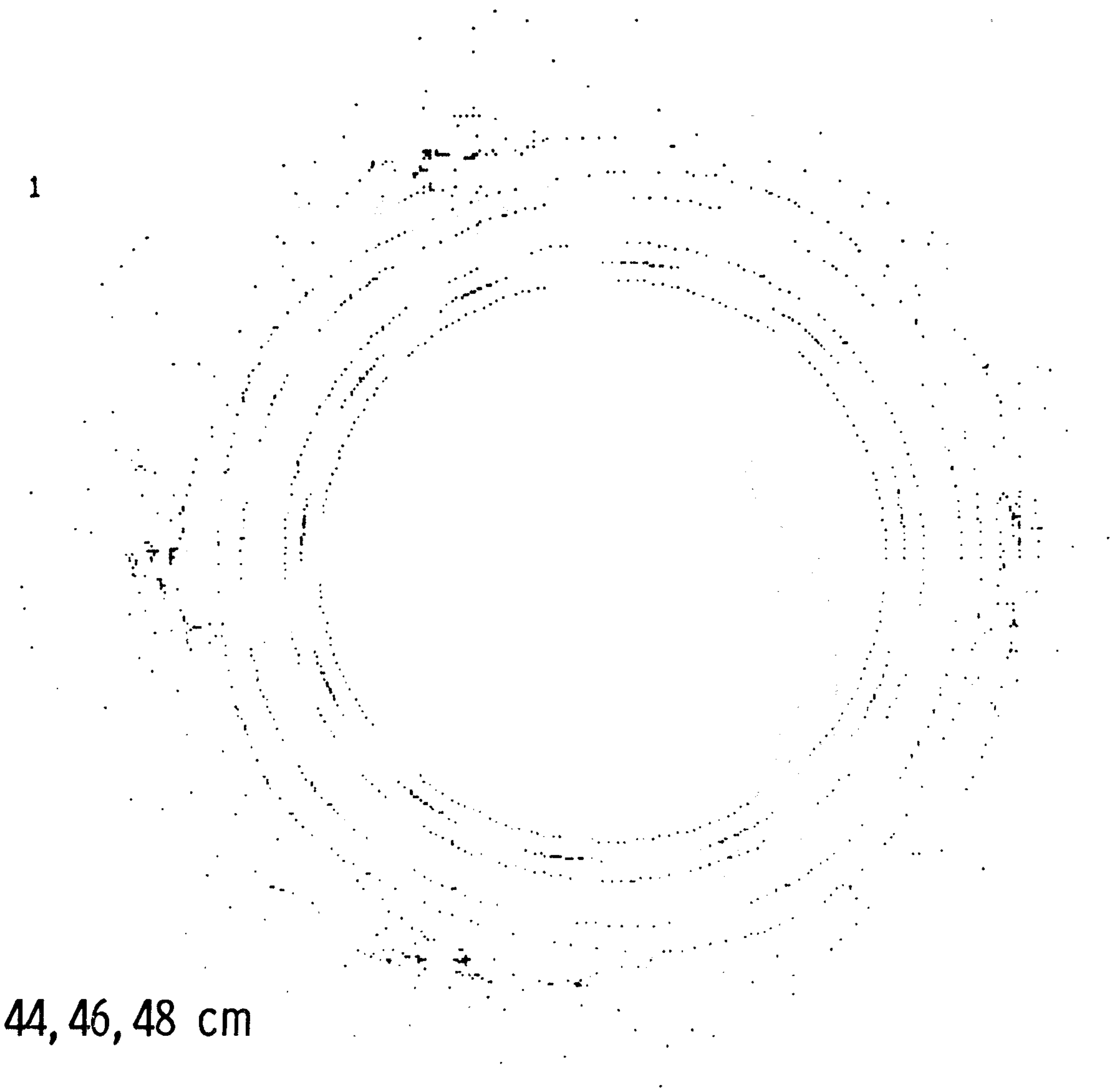

Fig. 10

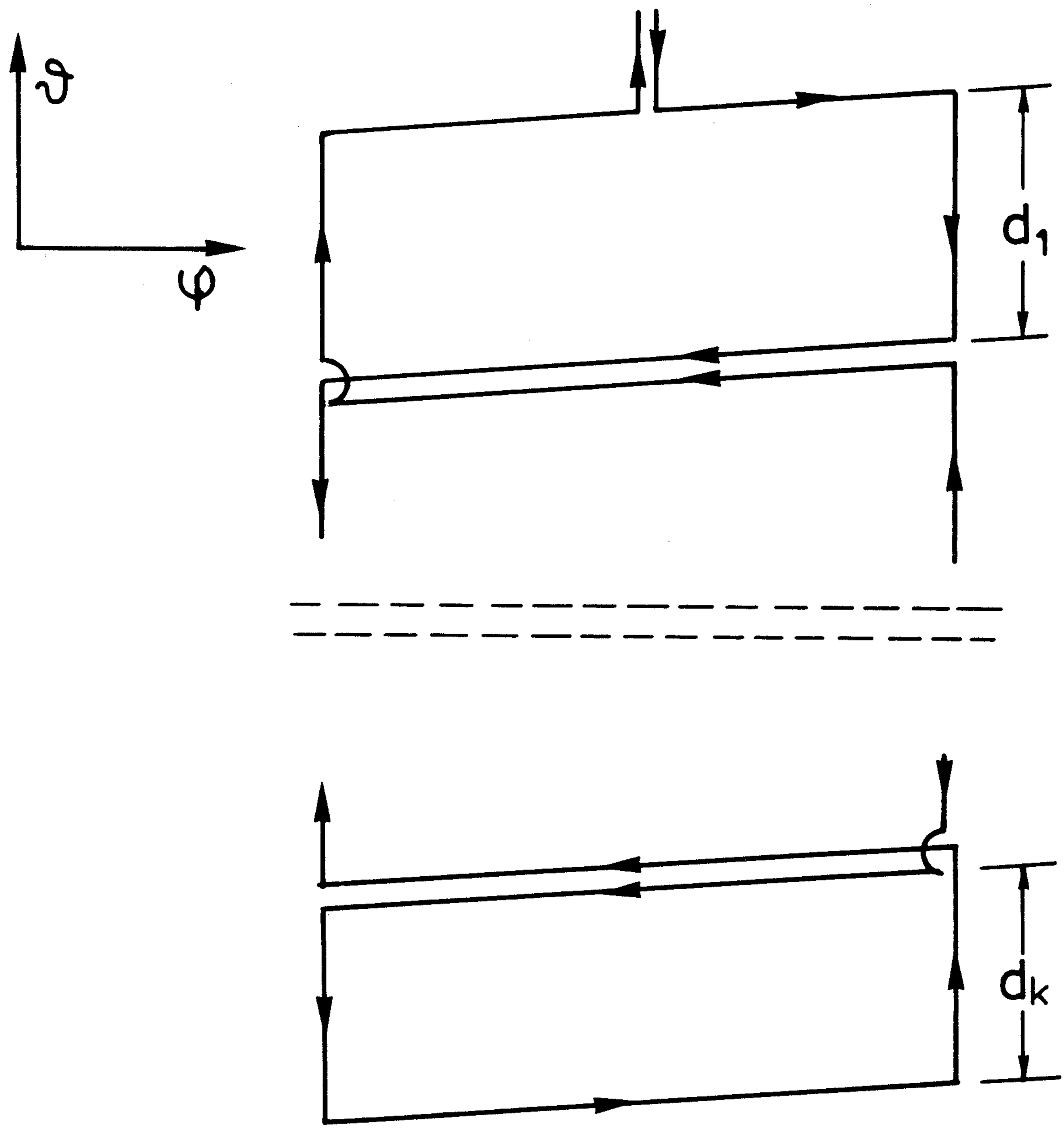

Fig. 11

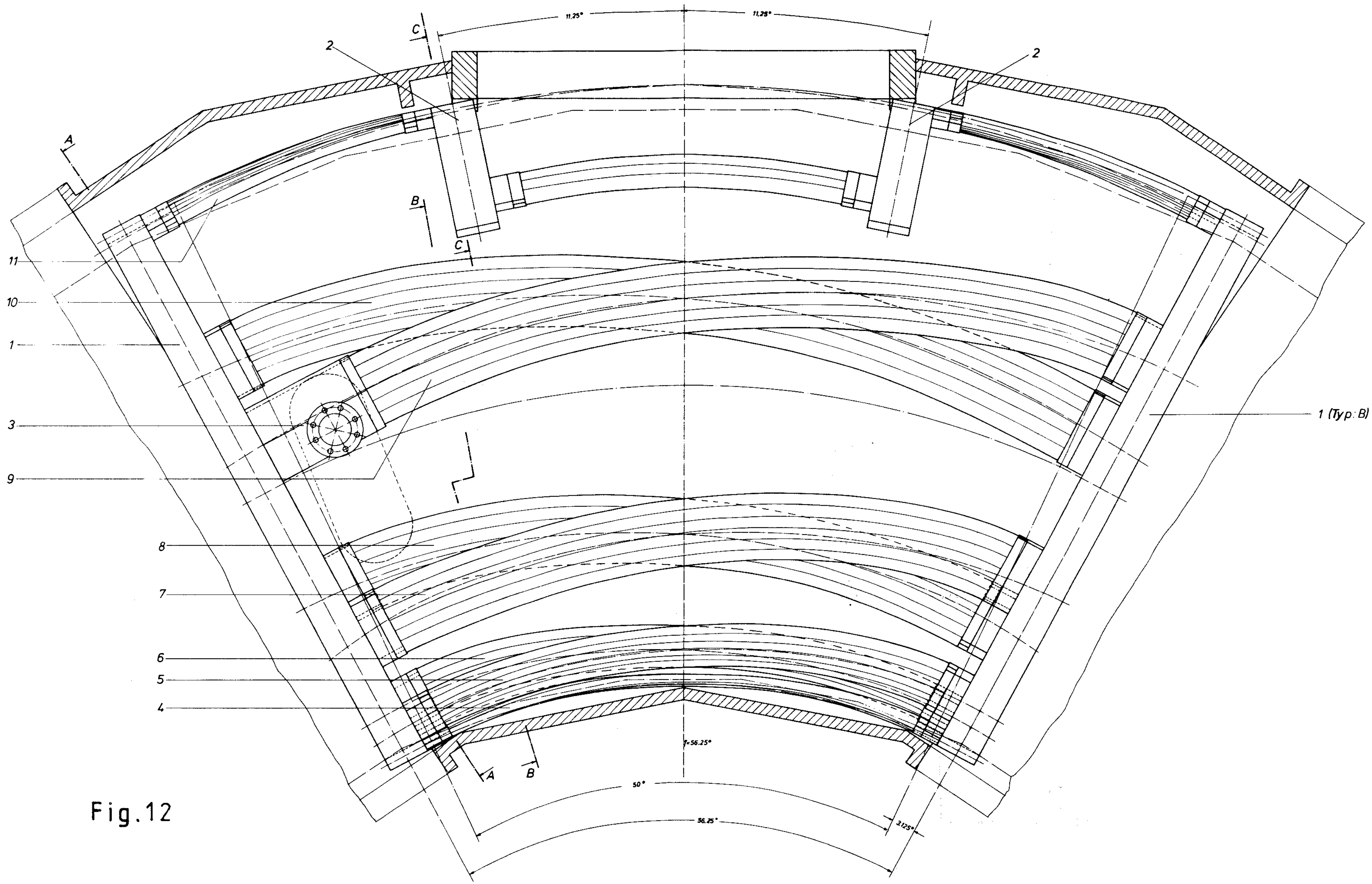

Fig.12

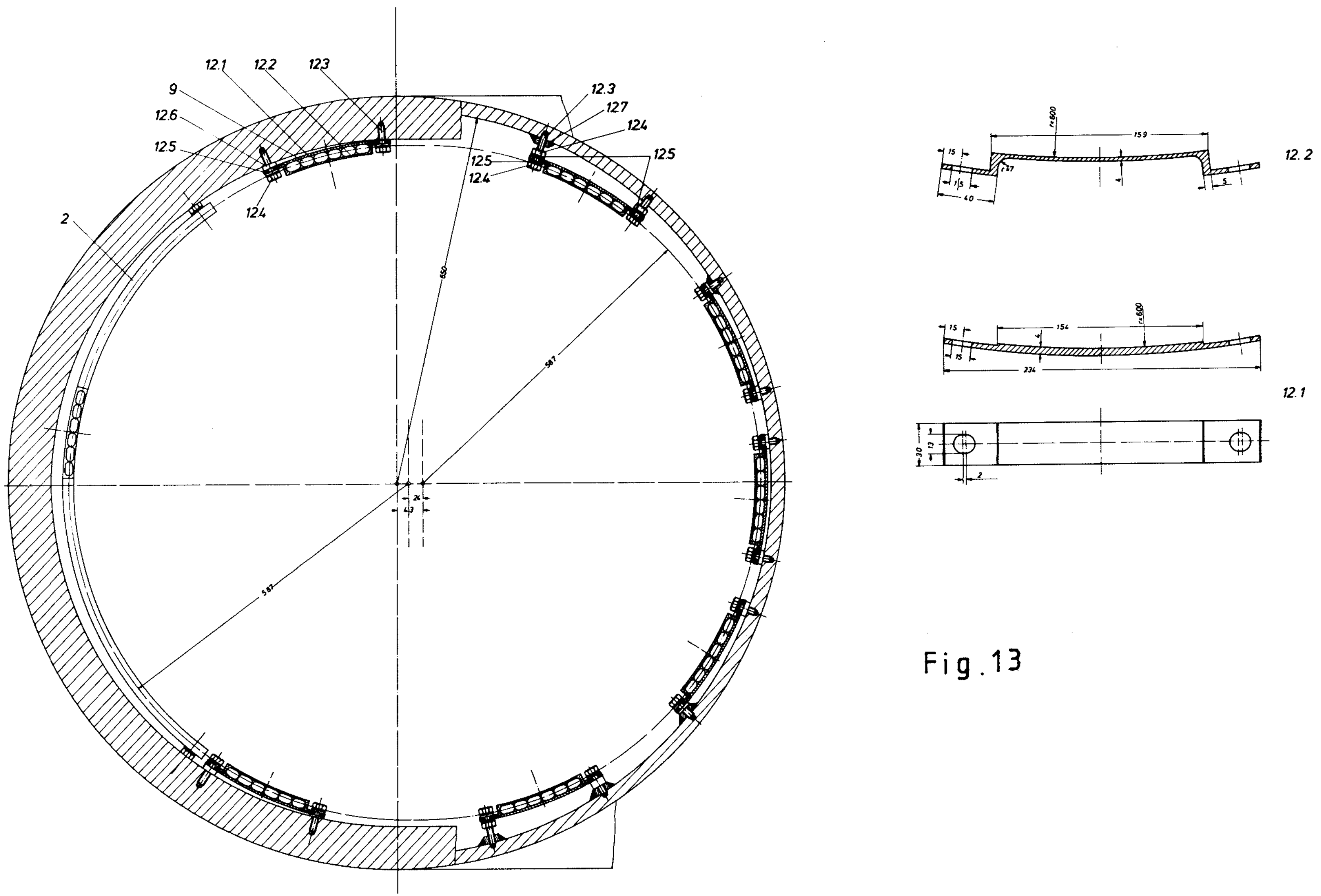

12.1
12.2
123
9
12.6
12.5
12.4
2
12.3
127
124
12.5
12.4
125
650
587
587
24
43
159
15
1|5
40
r=600
4
5
12. 2
15
154
r=600
15
4
234
12.1
30
12
2

Fig.13

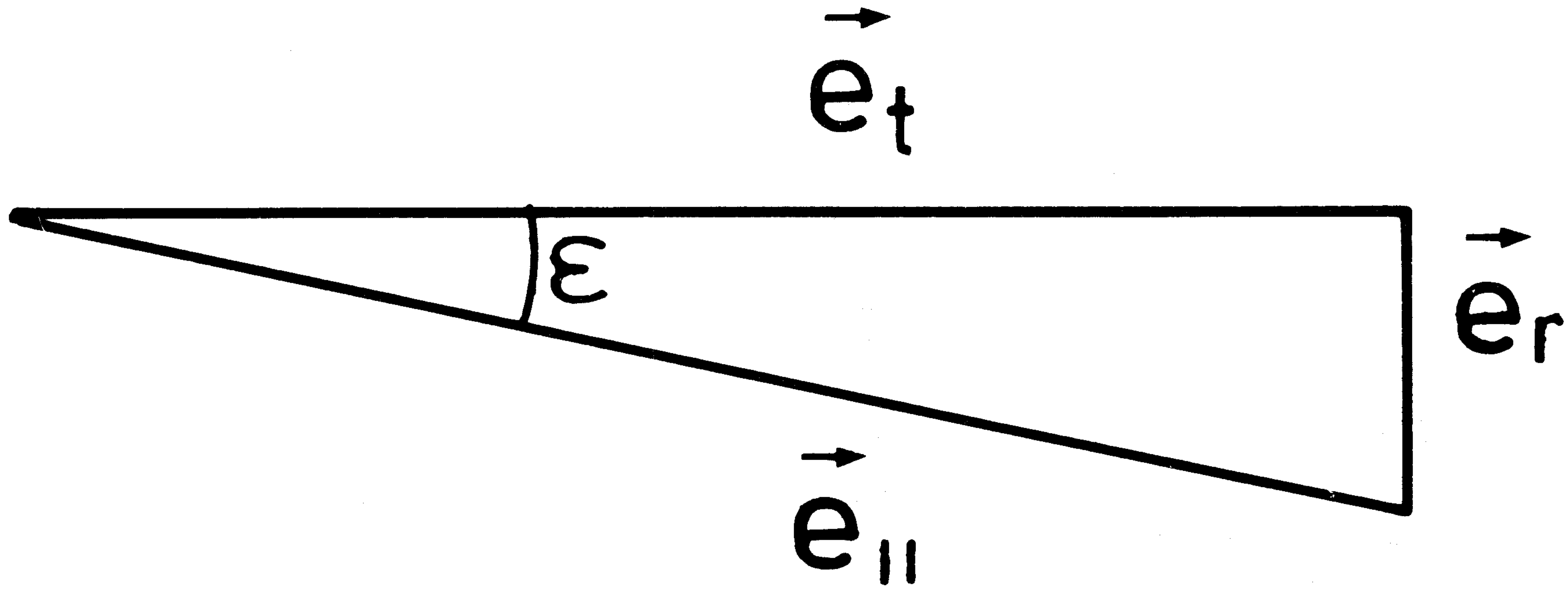

Fig. 14

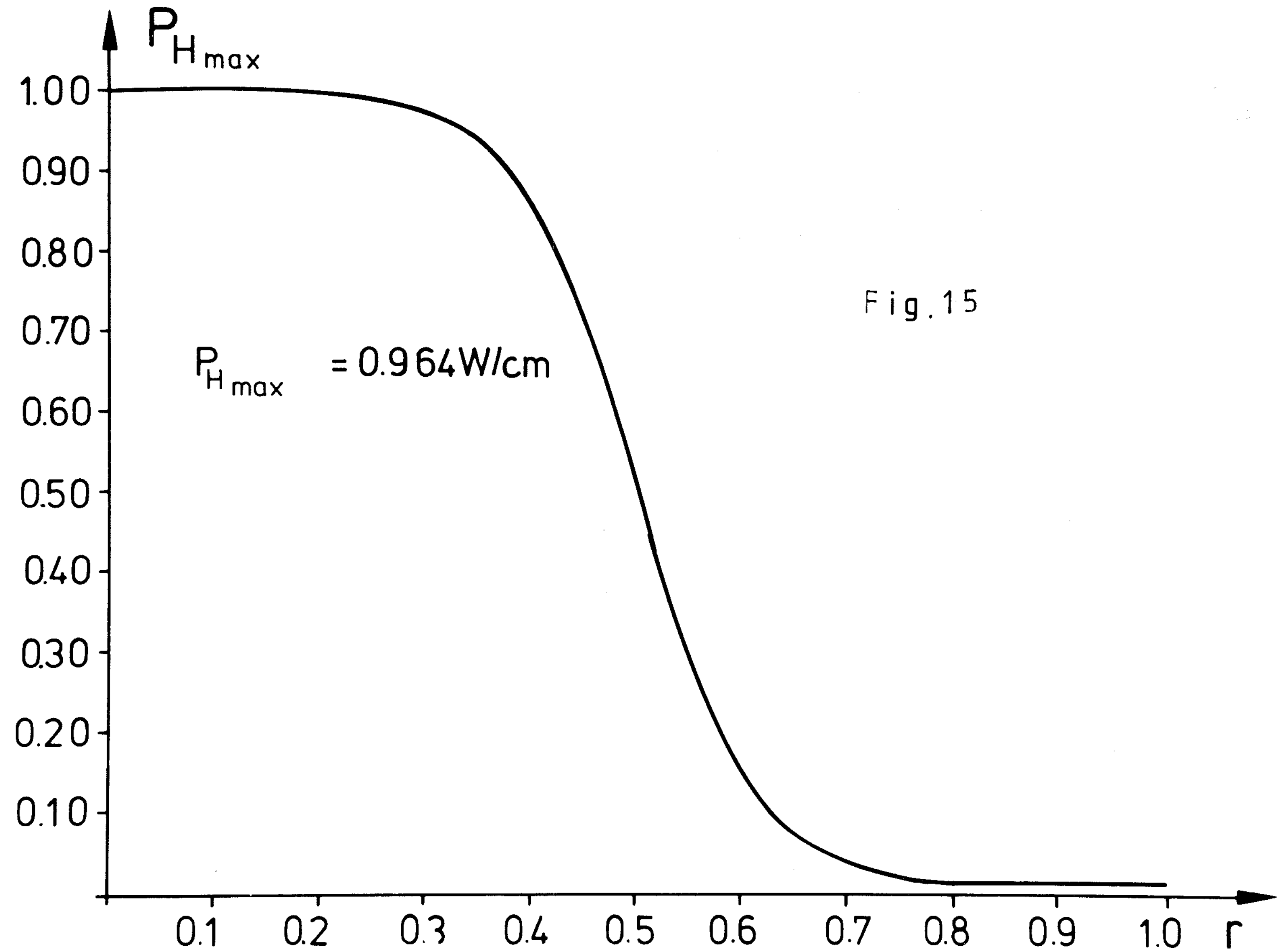
$P_{H_{max}}$
$P_{H_{max}} = 0.964 W/cm$
1.00
0.90
0.80
0.70
0.60
0.50
0.40
0.30
0.20
0.10
0.1
0.2
0.3
0.4
0.5
0.6
0.7
0.8
0.9
1.0
r

Fig. 15

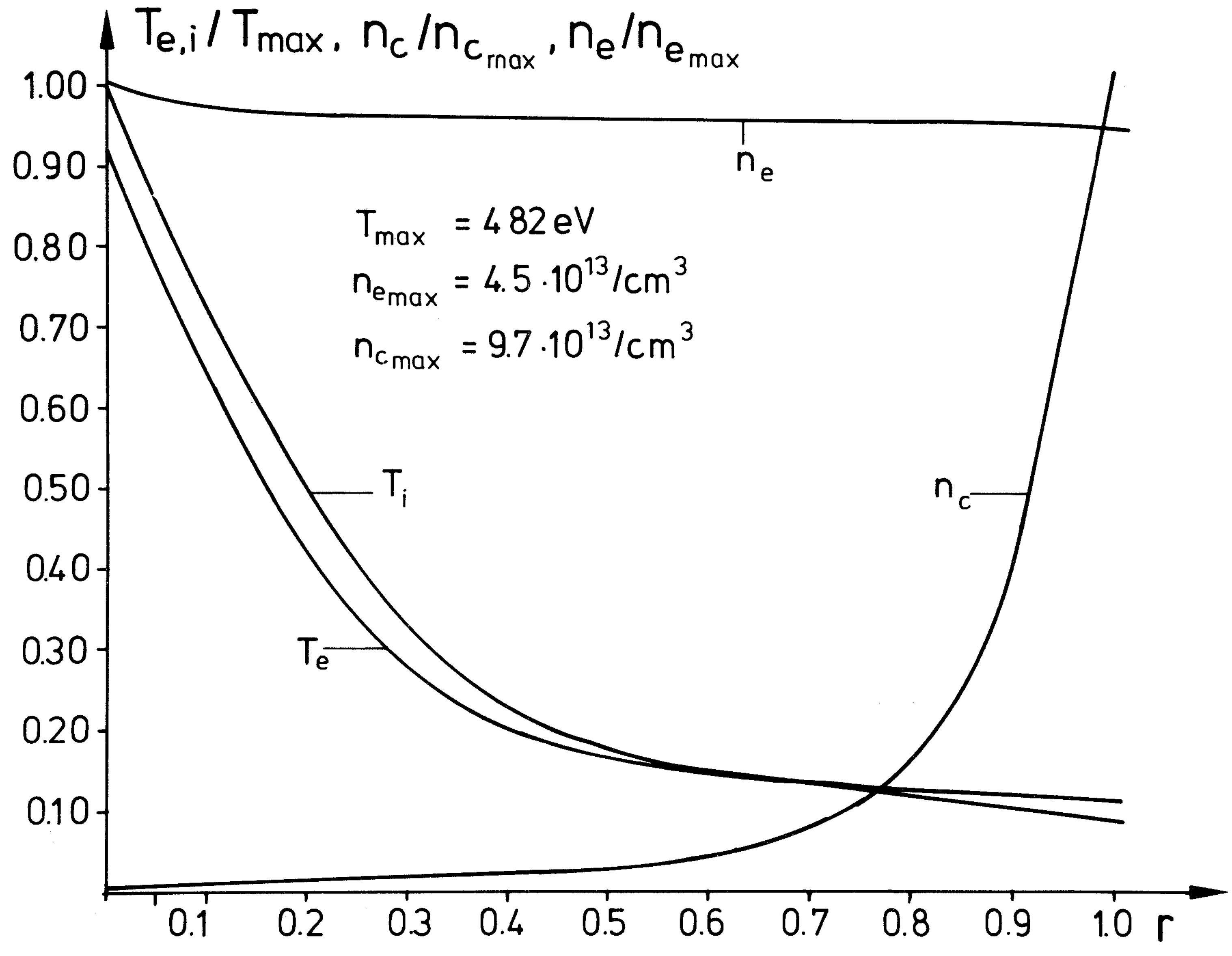

$T_{e,i}/T_{max}$, $n_c/n_{c_{max}}$, $n_e/n_{e_{max}}$
1.00
0.90
0.80
0.70
0.60
0.50
0.40
0.30
0.20
0.10
T_{max} = 4.82 eV
$n_{e_{max}} = 4.5 \cdot 10^{13}/cm^3$
$n_{c_{max}} = 9.7 \cdot 10^{13}/cm^3$
n_e
T_i
T_e
n_c
0.1
0.2
0.3
0.4
0.5
0.6
0.7
0.8
0.9
1.0
r

Fig. 16

$n_{e_{max}} = 1.19 \cdot 10^{14}/cm^3$

$n_{e_{min}} = 1.65 \cdot 10^{12}/cm^3$

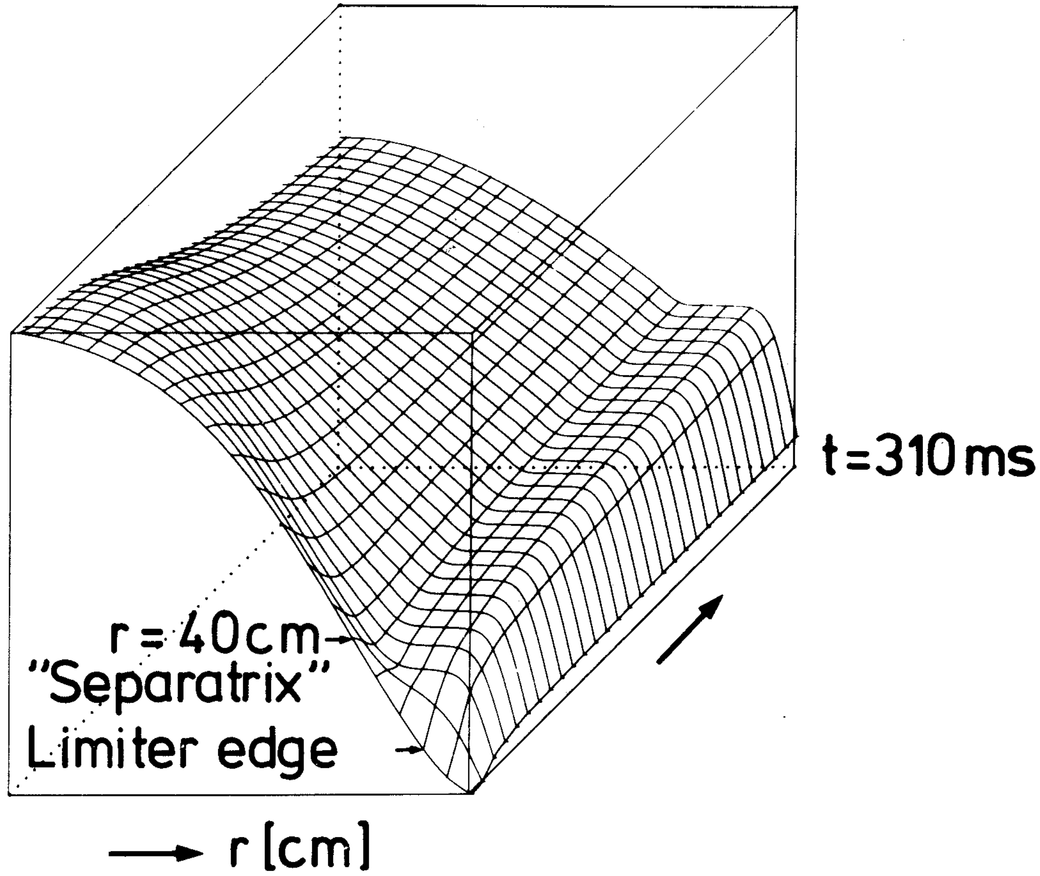

Fig. 17

$n_{e\,max} = 1.19 \cdot 10^{14}/cm^3$

$n_{e\,min} = 1.65 \cdot 10^{12}/cm^3$

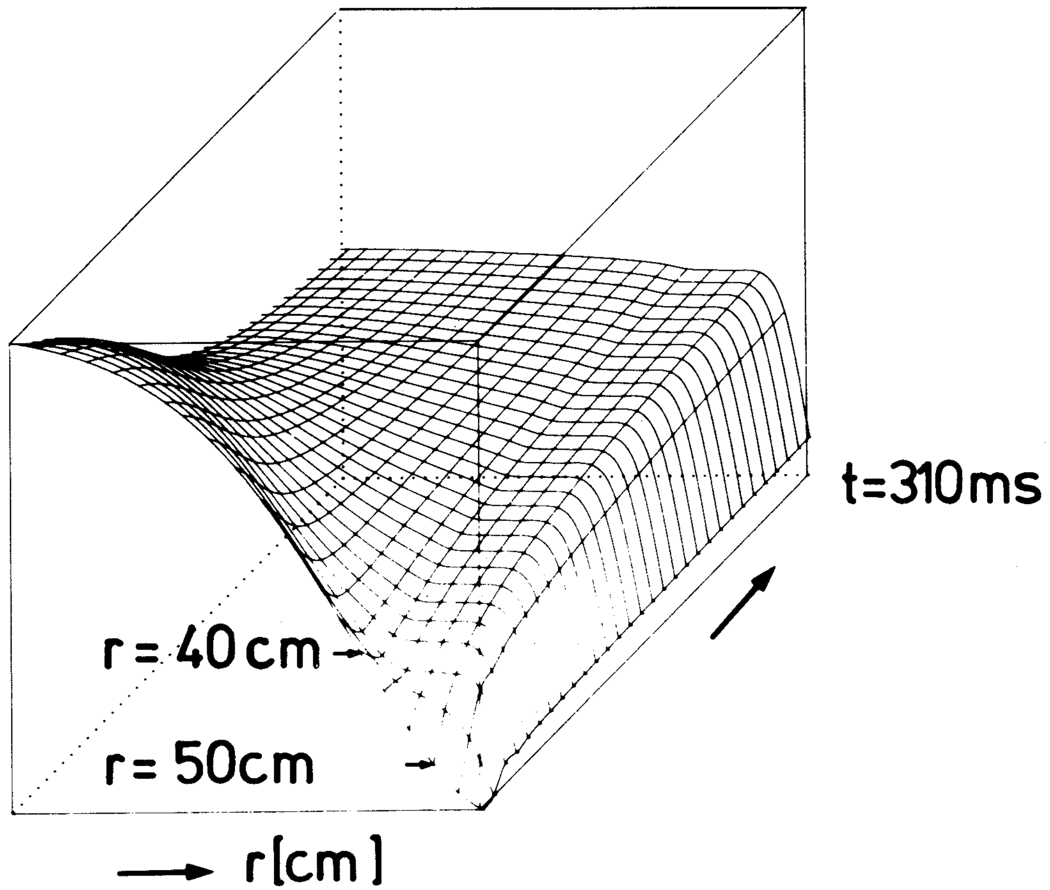

Fig. 18

$$B \cdot \{r, \vartheta\} = \{r + \Delta r\, \vartheta \cdot e^{-(\vartheta/12\pi)^2}, \vartheta\}$$

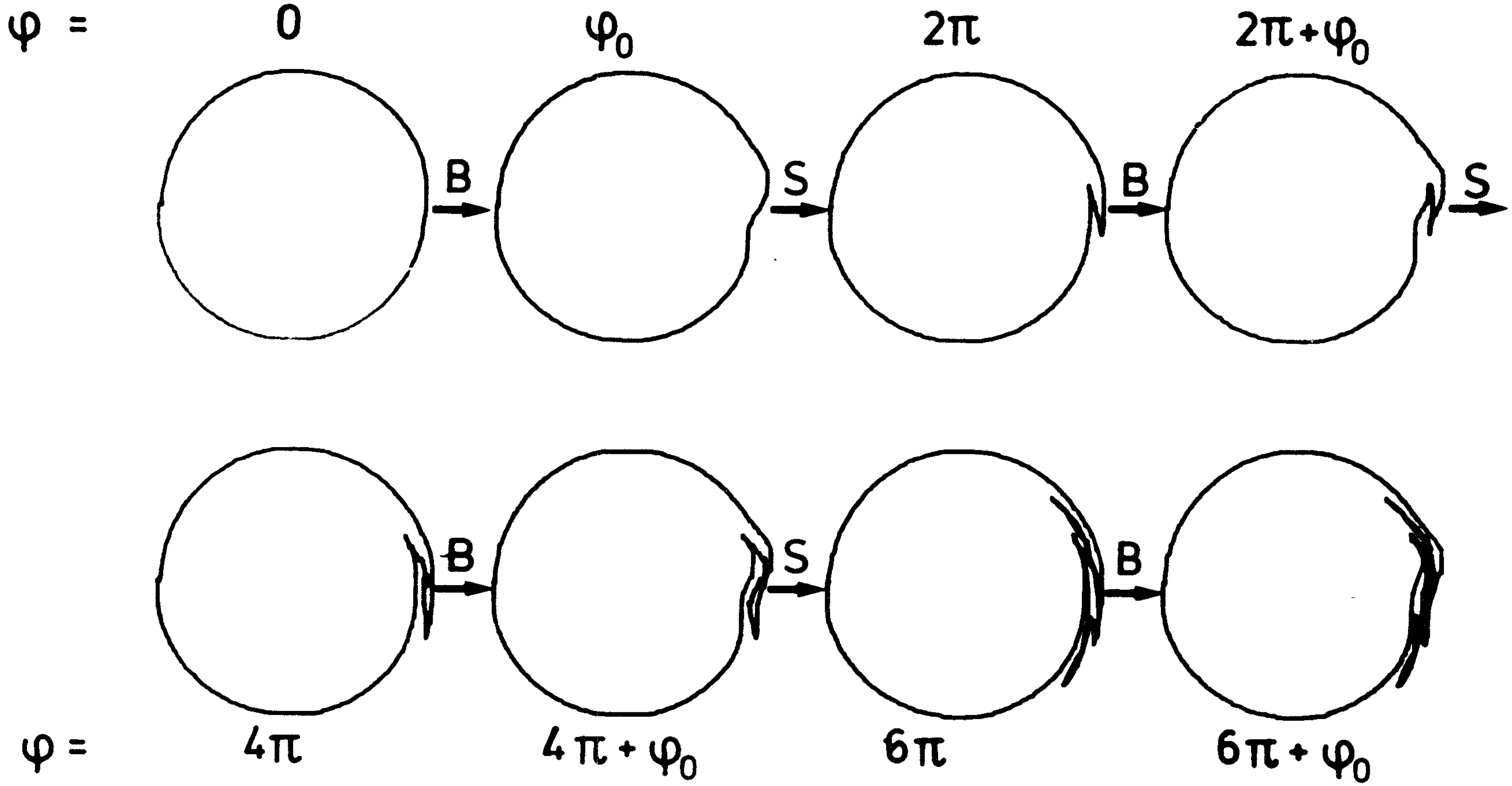

$$S \cdot \{r, \vartheta\} = \{r, \vartheta + 2\pi (r_0 - r)\}$$

Fig 19